Antimicrobial, antioxidant and cytocompatible coaxial wet-spun fibers made of polycaprolactone and cellulose acetate loaded with essential oils for wound care

Catarina Miranda, Elina Marinho, Catarina Leal Seabra, Camille Evenou, Jérôme Lamartine, Berengere Fromy, Susana P.G. Costa, Natália Homem, Helena Felgueiras

International Journal of Biological Macromolecules 277 (2024) 134565

Contents lists available at ScienceDirect

International Journal of Biological Macromolecules

journal homepage: www.elsevier.com/locate/ijbiomac

Antimicrobial, antioxidant and cytocompatible coaxial wet-spun fibers made of polycaprolactone and cellulose acetate loaded with essential oils for wound care

Catarina S. Miranda [a], Elina Marinho [a], Catarina Leal Seabra [b,1], Camille Evenou [c], Jérôme Lamartine [c], Berengere Fromy [c], Susana P.G. Costa [d], Natália C. Homem [e], Helena P. Felgueiras [a,*]

[a] Centre for Textile Science and Technology (2C2T), University of Minho, Campus of Azurém, 4800-058 Guimarães, Portugal
[b] Associate Laboratory for Green Chemistry (LAQV), Network of Chemistry and Technology (REQUIMTE), Department of Chemical Sciences, Faculty of Pharmacy, University of Porto, 4050-313 Porto, Portugal
[c] Équipe Intégrité fonctionnelle du tissu cutané (SKIN). Laboratoire de biologie tissulaire et d'ingénierie thérapeutique (LBTI), CNRS UMR5305, Université Lyon I, 7 passage du Vercors, 69367 Lyon Cedex 07, France
[d] Centre of Chemistry (CQ), University of Minho, Campus of Gualtar, 4710-057 Braga, Portugal
[e] Simoldes Plastics S.A., Rua Comendador António da Silva Rodrigues, 165, 3720-193 Oliveira de Azeméis, Portugal

ARTICLE INFO

Keywords:
Antimicrobial effectiveness
Core-shell fibers
Drug delivery system
Sustained release
Therapeutic natural extracts

ABSTRACT

Chronic wounds represent a serious worldwide concern, being often associated with bacterial infections. As the prevalence of bacterial infections increase, it is crucial to search for alternatives. Essential oils (EOs) constitute a promising option to antibiotics due to their strong anti-inflammatory, analgesic, antioxidant and antibacterial properties. However, such compounds present high volatility. To address this issue, a drug delivery system composed of coaxial wet-spun fibers was engineered and different EOs, namely clove oil (CO), cinnamon leaf oil (CLO) and tea tree oil (TTO), were loaded. Briefly, a coaxial system composed of two syringe pumps, a coagulation bath of deionized water, a cylindrical-shaped collector and a coaxial spinneret was used. A 10 % *w/v* polycaprolactone (PCL) solution was combined with the different EOs at 2 × minimum bactericidal concentration (MBC) and loaded to a syringe connected to the inner port, whereas a 10 % *w/v* cellulose acetate (CA) solution mixed with 10 % w/v polyethylene glycol (PEG) at a ratio of 90:10 % *v/v* (to increase the fibers' elasticity) was loaded to the syringe connected to the outer port. This layer was used as a barrier to pace the release of the entrapped EO. The CA's inherent porosity in water coagulation baths allowed access to the fiber's core. CA was also mixed with 10 % w/v polyethylene glycol (PEG) at a ratio of 90:10 % v/v (CA:PEG), to increase the fibers' elasticity.

Microfibers maintained their structural integrity during 28 days of incubation in physiological-like environments. They also showed high elasticities (maximum elongations at break >300 %) and resistance to rupture in mechanical assessments, reaching mass losses of only ≈ 2.29 % - 57.19 %. The EOs were released from the fibers in a prolonged and sustained fashion, in which ≈ 30 % of EO was released during the 24 h of incubation in physiological-like media, demonstrating great antibacterial effectiveness against *Staphylococcus aureus*, *Staphylococcus epidermidis*, *Escherichia coli* and *Pseudomonas aeruginosa*, the most prevalent bacteria in chronic wounds. Moreover, microfibers showed effective antioxidant effects, presenting up to 59 % of reduction of 2,2-diphenyl-1-picrylhydrazyl (DPPH) activity. Furthermore, the coaxial system was deemed safe for contact with fibroblasts and human keratinocytes, reaching metabolic activities higher than 80 % after 48 h of incubation. Data confirmed the suitability of the engineered system for potential therapeutics of chronic wounds.

* Corresponding author.
E-mail addresses: catarina.miranda@2c2t.uminho.pt (C.S. Miranda), elinamarinho@2c2t.uminho.pt (E. Marinho), cseabra@ff.up.pt (C.L. Seabra), camille.evenou@ibcp.fr (C. Evenou), jerome.lamartine@ibcp.fr (J. Lamartine), berengere.fromy@ibcp.fr (B. Fromy), spc@quimica.uminho.pt (S.P.G. Costa), natalia.homem@simoldes.com (N.C. Homem), helena.felgueiras@2c2t.uminho.pt (H.P. Felgueiras).
[1] Current affiliation: Agência Nacional de Inovação, Porto, Portugal.

https://doi.org/10.1016/j.ijbiomac.2024.134565
Received 21 March 2024; Received in revised form 29 July 2024; Accepted 5 August 2024
Available online 6 August 2024

1. Introduction

Chronic wounds are normally recognized by their inability to heal in an appropriate period of time, stalling at the inflammatory phase of the healing cascade [1]. This type of wound is considered a major threat to global health, being frequently associated with high mortality and morbidity rates [2,3]. They can greatly impact the health and quality of life of patients and their effects should not be underestimated. Bacterial infections are frequent in chronic wounds, resulting in the degradation of the wound tissue [4]. *Staphylococcus aureus*, *Staphylococcus epidermidis*, *Escherichia coli* and *Pseudomonas aeruginosa* represent four of the most prevalent bacteria in chronic wounds [2,3]. In fact, according to a systematic review between 2007 and 2018, the incidence of *E. coli* infections has been determined to be about 73,000 every year in the United States (USA), whereas *P. aeruginosa* caused around 51,000 healthcare-associated infections annually in the same country, as reported in a study conducted between 2011 and 2014 by the National Healthcare Safety Network (NHSN) [5,6]. Moreover, according to the Center for Disease Control and Prevention (CDC), the incidence of *S. aureus*-induced infections was of 119,000 during the year 2017 [7]. In addition, the World Health Organization (WHO) stated that during the year of 2020 that 7 out of 100 hospitalizations in developed countries were related with *S. epidermidis* infections [8].

Since the invention of penicillin, antibiotics have been commonly used as the first line of treatment for bacterial infections. Yet, their excessive use has increased the need for alternative solutions [9]. Essential oils (EOs) are plant-derived products and have been recognized as promising alternatives or co-adjuvant therapeutics for the treatment of bacterial infections [10,11]. Such compounds have shown effective antimicrobial, antioxidant and anti-inflammatory properties, without significant side effects compromising human health [12]. Examples of EOs that have gained considerable importance for fighting microbial pathogens are clove oil (CO), cinnamon leaf oil (CLO) and tea tree oil (TTO), which antimicrobial, antioxidant and anti-inflammatory properties have been addressed in many reports [13,14]. CO can be attained from the aromatic flower buds and leaves of *Eugenia caryophyllata*, which is mainly composed of eugenol (78 %), β-caryophyllene (13 %) and eugenol acetate. The various therapeutic effects of CO are due to the presence of eugenol that not only is considered a safe product, but also possesses exceptional antibacterial, antifungal, anti-inflammatory, as well as high analgesic and antioxidant properties [15]. CLO is extracted from cinnamon barks and leaves and is primarily composed of cinnamaldehyde. It displays similar biological traits to CO [16]. In addition, TTO is obtained from *Melaleuca alternifolia* and shows high antimicrobial properties due to its main component, terpinen-4-ol [17]. Despite their beneficial biological features, EOs may cause cytotoxic effects when present at higher concentrations and low stability in physiological-like media, besides presenting high volatility [11]. To overcome such limitations, EOs can be loaded onto polymeric structures, such as coaxial fibers produced via wet-spinning, that protect the compounds from the surrounding environment and allow their controlled, sustained release overtime without loss of biological functions [18].

Wet-spinning is a fiber producing technique involving the injection of a polymeric solution into a non-solvent coagulation bath, which results in a fast precipitation of the polymer and solvent removal, ultimately, forming solid microfibers. The generated fibers are characterized by possessing high porosities, wide rays of organizations, dimensions, physical and chemical properties, and for enabling cell infiltration and maturation when organized in scaffolding systems [18,19]. Many natural polymers, including alginate, gelatin, chitosan and cellulose have been processed by wet-spinning, resulting in fibers with a tunable variety of diameters and structural organizations [1]. Cellulose acetate (CA) is a cellulose modified polymer obtained through the modification of three hydroxyl groups per molecule of cellulose by an acetyl group. CA, being a polysaccharide as well, is mostly recognized by its high mechanical properties, moisture absorption and permeability, making it a promising polymer for medical uses [20]. Synthetic polymers, such as polylactic acid (PLA), polyglycolic acid (PGA), polyethylene glycol (PEG) and poly(ε-caprolactone) (PCL), have also been frequently used to generate wet-spun fibers [21]. PCL is a semi-crystalline polyester, endowed with good solubility, biocompatibility, biodegradability, a low melting point and excellent mechanical properties, also possessing a hydrophobic behavior. It is compatible with many other polymers, making it ideal for engineering scaffolds and implantable systems for biomedical applications [22]. Likewise, PEG is recognized as a potential material for such applications, since it displays high biocompatibility, non-toxicity, non-immunogenicity and has been approved by the Food and Drug Administration [23,24].

This work aims at producing coaxial wet-spun fibers as a different therapeutic solution for the treatment of chronic wounds, endowed with strong antibacterial and anti-oxidant properties, as well as good mechanical performances and high structural stabilities when exposed to physiological media. Such fibers were produced with a PCL core, to ensure fibers' structural integrity, mixed with the EOs CO, CLO and TTO, to endow the fibers with antibacterial properties [12,25]. The shell of the fibers was made of CA, generating a porous layer that allowed access to the core, combined with the plasticizer polyethylene glycol (PEG), for improving elasticity [26]. Although several research studies of wet-spinning can be found in literature, this project constitutes the first coaxial wet-spun fibrous system (with two layers) incorporating EOs, capable of effective antibacterial and anti-oxidant activities and effective mechanical performances. The morphology of the system was assessed by brightfield and scanning electron microscopy (SEM) and detailed analyses of mechanical and thermal properties were performed. Additionally, the structural resistance of the coaxial fibers to external agents present in the physiological media was investigated, along with the release profiles of the entrapped EOs. Several biological tests, including examinations of skin cell cultures, were also conducted to determine the safety of the engineered structure.

2. Materials and methods

2.1. Materials

CA (Mn 50,000), PCL (Mn 80,000), PEG (Mn 20,000), 1,1–diphenyl-2-picrylhydrazyl (DPPH), Dulbecco's Phosphate Buffered Saline (DPBS), Trypsin-EDTA, Tryptan Blue solution and Fetal Bovine Serum (FBS) were obtained from Sigma-Aldrich (St. Louis, Missouri, USA). *N,N*-dimethylformamide (DMF) was acquired from Merck (Darmstadt, Germany). Dimethyl sulfoxide (DMSO) and 6-hydroxy-2,5,7,8-tetramethylchroman-2-carboxylic acid (Trolox) were acquired from Fisher (Maharashtra, India). Dulbecco's Modified Eagle Medium (DMEM), Penicillin-streptomycin, Alamar Blue and LDH kit were acquired from Invitrogen (Massachusetts, USA). Triton was acquired from Bio-Rad Laboratories (California, USA). Pure cinnamon leaf oil (CLO, ρ = 1.049), pure clove oil (CO, ρ =0.900) and pure tea tree oil (TTO, ρ = 0.895) were obtained from Folha d'Água Company (Santo Tirso, Portugal). Sodium phosphate dibasic (Sigma-Aldrich), monosodium phosphate monohydrate (Merck), potassium chloride (Merck) and sodium chloride (Merck) were used in the preparation of phosphate buffer saline solution (PBS at 0.1 M: 1.44 g/L of Na_2HPO_4, 0.24 g/L of KH_2PO_4, 0.20 g/L KCl and 8.00 g/L of NaCl, adjusted to physiological pH 7.4). Gram-positive bacteria *S. aureus* (ATCC 6538) and *S. epidermidis* (ATCC 35984), along with Gram-negative bacteria *E. coli* (ATCC 25922) and *P. aeruginosa* (ATCC 25853) were supplied by American Type Culture Collection (ATCC, Virginia, USA). For bacteria growth, trypticase soy broth (TSB), trypticase soy agar (TSA), nutrient agar (NA) and nutrient broth (NB) were purchased from VWR (Alfragide, Portugal), while Mueller Hinton broth (MHB) was obtained from CondaLab (Madrid, Spain). Human keratinocytes cell line (HaCaT) was purchased from Thermo Fischer Scientific (Waltham, USA) and mouse embryonic fibroblasts cell line (NIH 3 T3) from Sigma Aldrich (Darmstadt, Germany).

All reagents were used without further purification.

2.2. Determination of EOs minimum inhibitory and bactericidal concentrations (MIC and MBC)

CO, CLO and TTO MICs against *S. aureus, S. epidermidis, E. coli* and *P. aeruginosa* were determined using the broth microdilution method [27], which adapts the standard published by the Clinical and Laboratory Standards Institute (CLSI) and the European Committee on Antimicrobial Susceptibility Testing (EUCAST) [28].

Prior to any testing, the chemical compositions of the CO, CLO and TTO were assessed by solid-phase micro-extraction and gas chromatography–mass spectrometry (SPME-GC–MS). Here, a SPME fiber of polydimethylsiloxane was exposed to the vapor phase of the EOs, at 1 mg/mL, for 24 h at 35 °C. Stock solutions of CO, CLO and TTO were prepared at concentrations of 528, 524.50 and 447.50 mg/mL, respectively. 100 μL of each solution were added to the first column of a 96-well plate (3 replicates). Serial dilutions (1/2 *v*/v) were performed in MHB, until a final volume of 50 μL was achieved in each well. The bacterium suspension prepared in MHB at 1×10^6 colony forming units (CFUs)/mL was then added to the wells (50 μL; final bacterium concentration of 5×10^5 CFUs/mL). As control, MHB (negative) and the bacterial suspensions free from CO/CLO/TTO (positive) were used. An EZ READ 2000 Microplate Reader (Biochrom, Harvard, USA) was used to read absorbances at 600 nm, before and after the 24 h incubation period at 37 °C and 120 rpm. MIC was identified by differences in absorbance readings. The MBC was determined by culturing the bacterial solution at MIC and its vicinities (before and after MIC value). To accomplish that, aliquots were collected, serially diluted in PBS (10^1 to 10^4), plated in TSA (*S. aureus, S. epidermidis* and *E. coli*) and NA (*P. aeruginosa*), and then incubated at 37 °C for 24 h, at which point grown colonies were observed and counted.

2.3. Wet-spun fibers production

10 % *w/v* CA, PEG and PCL solutions were prepared, separately, in DMF and stirred continuously for 1 h at 50 °C. PEG was added to a portion of the CA solution at a ratio of 10:90 *v*/v, respectively, and homogeneously blended for 12 h at 50 °C (CA-PEG solution). On its turn, CO, CLO and TTO were combined with the PCL solution at 2× their MIC and left to homogenize for 1 h at 50 °C (PCL-CO, PCL-CLO and PCL-TTO solutions). Viscosities were measured using a viscometer Brookfield DV-II + Pro (Boston, USA), spindle 21, with speeds of 50–70 rpm at 17–35 °C. Air bubbles were removed by solutions' ultrasonication, followed by fiber production. The rate and volume of extrusion were tuned by two syring pumps (NE-300, New Era Pump Systems, Norleq, Santo Tirso, Portugal). The system was also composed by a coaxial spinneret and a large tray containing 500 mL of deionized water (dH_2O) coagulation bath, at room temperature (RT). All fibers were collected automatically in a cylindrical-shaped collector at speeds of 9–13 rpm and dried for 1 h at RT. Syringes connected to the inner port (core) and the outer port (shell) of the coaxial spinneret were loaded with PCL-CO, PCL-CLO, PCL-TTO solutions and CA-PEG solution, respectively. PCL-CO, PCL-CLO and PCL-TTO were ejected at 0.10 mL/min, whereas CA-PEG was ejected at 0.12 mL/min, forming PCL-CO/CA-PEG, PCL-CLO/CA-PEG and PCL-TTO/CA-PEG fibers. Control fibers were produced without the shell (just PCL,PCL-CO, PCL-CLO and PCL-TTO), without the core (hollow fibers of CA and CA-PEG) and without some of the components of the coaxial system, namely CO,CLO,TTO and PEG (PCL/CA), PEG (PCL-CO/CA, PCL-CLO/CA and PCL-TTO/CA), and CO,CLO and TTO (PCL/CA-PEG). The same processing parameters were applied for both control samples and the complete system. Finally, all samples were stored in a cabinet desiccator (Sicco, Grünsfeld, Germany) at 19 °C and a relative humidity of 41 %, for additional testing.

2.4. Microfibers' physical, chemical, thermal and mechanical characterization

2.4.1. Brightfield microscopy

Brightfield microscopy was applied to analyze the morphology of all fiber typologies. An inverted Leica DM IL LED microscope (Leica microsystems, Weetzlar, Germany) was used and five images were collected at 5× and 10× magnifications. In addition, the average fiber thicknesses (5 measurements per image) were determined via ImageJ® software (version 1.53, National Institutes of Health, Bethesda, Maryland, USA).

2.4.2. Scanning electron microscopy (SEM)

Morphological analyses were done in an Ultra-high Resolution Field Emission Gun Scanning Electron Microscope (FEG-SEM), NOVA 200 Nano SEM, FEI Company (California, USA). Transversal section of samples was obtained by cryogenic cutting in liquid nitrogen using a microtome blade. Morphology of those transversal sections was obtained with a Secondary Electron Detector (SE) using an acceleration voltage of 10 kV. Before morphological analyses, samples were covered with a film of Au—Pd (80–20 wt%) of 30 nm using a high-resolution sputter coater, 208HR Cressington Company, coupled to a MTM-20 Cressington High Resolution Thickness Controller. Images were collected with a magnification of 500× and processed with Image J® software.

2.4.3. Attenuated total reflectance-fourier transform infrared spectroscopy (ATR-FTIR)

ATR-FTIR analyses were carried out with an IRAffinity-1S (Shimadzu, Kyoto, Japan), coupled with a HATR 10 accessory containing a diamond crystal, in order to characterize the chemical composition of all wet-spun fibers. Spectra were obtained between 400 and 4000 cm^{-1}, with 200 scans and 2 cm^{-1} resolution.

2.4.4. Differential scanning calorimetry (DSC)

The thermal stability of the samples was assessed by DSC analyses, with the use of a Mettler Toledo equipment model DSC-822 (Columbus, USA). The preparation of the samples was based on their placement in an aluminum crucible, being were exposed to a heating gradient of 10 °C/min, from 25 to 500 °C, under nitrogen atmosphere at 100 mL/min.

2.4.5. Thermogravimetric analysis (TGA)

TGA analyses were performed with a STA 7200 Hitachi (Fukuoka, Japan), in which the samples were placed in aluminum crucibles. The temperature ranged from 25 to 500 °C and samples were exposed to a heating gradient of 10 °C/min, under a nitrogen purge flow at 200 mL/min.

2.4.6. Mechanical performance

The mechanical performance all fiber samples was evaluated by determining their maximum elongations at break, using a Housefield H5KS dynamometer (Artilab, Kerkdriel, Netherlands). Such equipment was associated with the QMAT Materials Testing & Analysis software, following the standard ISO 2062–2009. Filaments of 10 cm in length from each sample were analyzed at RT with a holding distance (gauge length), starting at 100 mm, increasing until reaching the fibers' maximum elongation at break. The crosshead speed was established at 25 mm/min, using a loading cell of 2.5–250.0 N, applied with a load range of 5 N and a pre-load of 0 N.

2.4.7. Degree of swelling (DS)

Hydration properties of the fibers were assessed by calculating the fibers DS. Initially, 10 mg from each fiber typology were incubated in PBS at 37 °C. Such samples were weighted before and after 72 h immersion (at which point saturation was reached). DS was calculated using the following expression (Eq. 1):

$$DS\ (\%) = \frac{ws - wd}{wd} \times 100, \quad (1)$$

in which *ws* represents the weight of the swollen fibers (wet state) after each incubation period and *wd* represents the weight of the fibers in their dried state, prior to PBS immersion.

2.4.8. Fiber degradation

Fibers' structural integrity when exposed to physiological media was assessed by the incubation of 10 mg from each fiber typology in PBS, at 37 °C up to 28 days. In parallel, media were exchanged every week. After 1, 3, 7, 14, 21 and 28 days of incubation, samples were weighted. Mass loss was determined using the following expression (Eq. 2):

$$mass\ loss\ (\%) = \frac{mi - mf}{mi} \times 100, \quad (2)$$

in which *mi* (mg) represents the weight of the hydrated fibers at time 0 h (prior to fibers' incubation in PBS) and *mf* (mg) corresponds to the fibers' weight after each incubation period.

2.5. Release kinetics

The release kinetics of EOs were analyzed by UV–visible spectroscopy, using a UV-1800 UV–visible spectrophotometer (Shimadzu, Kyoto, Japan). Firstly, calibration curves relating to TTO (0.10 to 1.60 mg/mL), CLO (0.02 to 0.20 mg/mL) and CO (0.03 and 0.30 mg/mL) dissolved at different concentrations in PBS were elaborated, thus and enabling a reliable detection of the spectra's region of interest (220 nm for TTO and 280 nm for CO and CLO). Results were plotted as absorbance vs wavelength. Afterwards, CO, CLO and TTO release from all wet-spun fibers during time was assessed in PBS. Samples of 10 mg from each EOs-loaded fibers were incubated in 1 mL of PBS at 37 °C and 120 rpm up to 24 h. After 1, 2, 4, 6, and 24 h, aliquots of 150 μL were collected and their absorbances were measured via UV–visible spectroscopy, using a quartz microcuvette of 1.4 mL. The release of the EOs was determined by the differences in absorbance between the first moment of interaction (0 h) and the subsequent measuring periods up to 24 h.

2.6. Antioxidant activity analysis

Free radical-scavenger activity was determined using the 1,1-diphenyl-2-picrylhydrazyl (DPPH) assay. Samples of 10 mg were immersed in 1 mL of absolute ethanol and incubated at 37 °C and 120 rpm for 1, 2, 4, 6 and 24 h. Ethanol was selected because of the high solubility of EOs in such solvent, thus facilitating detection of their antioxidant activity (PBS leads to phase separation, which compromises absorbance readings) [29]. Aliquots were collected at each time period and, in a 96-well plate, 140 μL of a DPPH stock solution (400 μM in absolute ethanol) were mixed with 10 μL of each aliquot. DMSO and Trolox were used as negative and positive controls, respectively. The absorbances were monitored every 5 min for 1 h, and measured at 515 nm, using an EZ Read 2000 Microplate Reader. Experiments were conducted in triplicate and data was reported in terms of the percentage of reduced DPPH at a steady state, which was calculated as follows (Eq. 3):

$$DPPH_r\ (\%) = \frac{Ai - Ar}{Ai} \times 100, \quad (3)$$

in which *Ar* represents the absorbance registered at a steady state and *Ai* corresponds to the initial absorbance.

2.7. Bacteria inhibition: Time-kill kinetics

Antibacterial properties of all wet-spun fibers were evaluated by time-kill kinetics tests, which were performed according to standard ASTM E2149–01, adapted as reported previously [30]. The antibacterial profile of the wet-spun fibers was tested against 1×10^5 CFUs/mL suspensions of *S. aureus*, *S. epidermidis* and *E. coli* in TSB, along with suspensions of *P. aeruginosa* in NB. 10 mg samples from each fiber typology were placed in 1 mL of each bacterium suspension and incubated at 37 °C and 120 rpm for 1, 2, 4, 6 and 24 h. At each time point, bacterial suspensions were serially diluted in PBS (10^1 to 10^4), plated in TSA and NA, and incubated at 37 °C for 24 h. Grown colonies were counted, and results were expressed in in % of inhibition of four bacteria activities (*S. aureus*, *S. epidermidis*, *E. coli* and *P. aeruginosa*). All measurements were performed in triplicate.

2.8. Cytocompatibility testing

2.8.1. Cell culture conditions

The cytocompatibility and cell proliferation of all fiber typologies towards mouse embryonic fibroblast cell line (NIH 3 T3) and human keratinocytes cell line (HaCaT) were evaluated using direct contact assay. Cells were thawed and sub-cultured in DMEM supplemented with 10 % *v*/v inactivated FBS (30 min, 56 °C) and 1 % v/v penicillin-streptomycin, at 37 °C in a humidified atmosphere of 5 % CO_2. Thereafter, cells were chemically detached from cell culture flasks using trypsin-EDTA solution. The number of cells was determined using a Malassez cell (Marienfeld, Germany), with cells labelled with trypan blue (Sigma Aldrich, UK), and counted using a Carl Zeiss Suzhou Co., Ltd. (Suzhou, China) microscope. Cells were seeded in 96-wells plates (Greiner, Germany) and incubated for 24 h at 37 °C in a humidified atmosphere of 5 % CO_2. The experiments were performed using fibroblasts at passages 2 to 12 and keratinocytes cell line at passages 20 to 30. 2 mg of fibrous samples, corresponding to ≈ 1.20 cm length, were used for each test. Experiments were conducted in triplicate. Fibers were washed and disinfected during 5 min, 3 times with dH_2O and 1 time with ethanol 70 % *v*/v, respectively, prior to any testing.

2.8.2. Cell viability assessment

Prior to any fiber testing, the determination of the optimum cell number was carried out by seeding cells into 96-wells plates at concentrations from 5×10^3 to 2.5×10^4 cells/well. Cells were incubated overnight at 37 °C and 5 % CO_2 atmosphere. Afterwards, the medium was aspirated from all wells and 100 μL of a 10 % *v*/v alamar blue solution (Invitrogen) were added to each well. Cells were again incubated for 1 h and the fluorescence was read ($\lambda_{ex} = 560$ and $\lambda_{em} = 590$ nm) using Tecan fluorimeter (Tecan Spark, Lyon, France) with Tecan Spark Control 3.2 software. The metabolic activity for each cell concentration was calculated using Eq. 4:

$$Metabolic\ activity\ (\%) = \frac{Flu\ sample - Flu\ negative\ control}{Flu\ positive\ control - Flu\ negative\ control} \times 100, \quad (4)$$

where Flu sample corresponds to the fluorescence of each sample, Flu negative control corresponds to cells grown in 5 % v/v DMSO solution and Flu positive control corresponds to a seeding of 5×10^4 cells/well.

After determining the optimum cell number for each cell line (2×10^4 cells/well and 1.5×10^4 15,000 cells/well for NIH 3 T3 and HaCaT, respectively), cells were then seeded at the established optimum concentration and 6 h later, fibers were added to the wells. After 24/48 h of incubation at 37 °C and 5 % CO_2 atmosphere, the metabolic activity of the cells was evaluated, repeating all the procedures reported above.

2.8.3. Cell lysis assessment

Cell lysis test was performed by following the instructions from LDH kit (Invitrogen). Firstly, the optimum cell number for performing LDH assay was determined by seeding cells at concentrations from 0 to 1×10^4 cells/well in 96-well fat black tissue plates (6 replicates for each cell concentration). Cells were incubated overnight at 37 °C and 5 % CO_2

atmosphere. Afterwards, 10 μL of sterile water were added to the first three replicates of each cell concentration (spontaneous LDH activity), whereas 10 μL of 2 % *v*/v Triton solution in DPBS were added to the second set of replicates for each cell concentration (maximum LDH activity). Cells were again incubated for 45 min, protected from light, followed by the transfer of 50 μL of each supernatant to a new plate, to which 50 μL of a reaction mixture was added. Cells were once more incubated at RT during 10 min, protected from light. Then, 50 μL of a stop solution were added to all wells and fluorescence was read (λ_{ex} = 560 and λ_{em} = 590 nm) using Tecan fluorimeter. The fluorescence of the maximum LDH release activity absorbances minus the spontaneous LDH release absorbances versus the tested cell numbers was plotted with the GraphPad Prism 8.0 software.

Cells were then seeded at the determined optimum cell number and, 6 h later, fibers were added. After 24 h of incubation, the cell lysis test was repeated. The percentages of cell lysis were then determined using the following Eq. 5:

$$\textit{Cell lysis}\ (\%) = \frac{\textit{Fluo sample} - \textit{Fluo spontaneous ctrl}}{\textit{Fluo maximum ctrl} - \textit{Fluo spontaneous ctrl}} \times 100, \qquad (5)$$

where Fluo sample corresponds to the fluorescence of cells treated with each fibrous sample, Fluo spontaneous ctrl corresponds to cells treated with sterile H_2O (spontaneous LDH activity) and Fluo maximum ctrl corresponds to the cells treated with 2 % *v*/v Triton (maximum LDH activity).

2.8.4. Cell morphology observations

Cells morphologies were visualized with a light microscope (Carl Zeiss Suzhou Co., Ltd.). Light microscope images were collected at the beginning of the experiment (t = 0 h) and after 24 h of incubation in contact with each fibrous samples, as to evaluate the cell morphology, as well as the possible presence of damaged areas. The images were acquired at a 10× magnification objective using an Axiocam 105 color camera (Zeiss, Switzerland), with Zeiss ZEN 3.8 software.

2.9. Statistical analysis

All measurements were conducted in triplicate unless otherwise referred in the experimental sections. Numerical data were reported as mean ± standard deviation (SD). Data were treated using GraphPad Prism 8.0 Software (GraphPad Software Inc., USA). Normality analysis was performed, and results were analyzed using One-way ANOVA and Tukey multiple comparisons test, comparing the mean of each column with the mean of every other column. Statistically significant differences were considered at $p < 0.05$.

3. Results and discussion

3.1. Characterization of the EOs

Three different EOs (Table 1) were selected and tested in free form (not incorporated in fibers) for their MBCs against four bacteria commonly present in chronic wounds, namely *S. aureus*, *S. epidermidis*, *E. coli* and *P. aeruginosa* [2,3]. TTO was the most effective EO against all four bacteria. Several studies exploring TTO-loaded structures have reported this EO strong antibacterial effects as a result of the presence of 1,2,3,5-tetramethylbenzene, along with terpinen-4-ol (Table S1 in Supporting Information) [14,31]. Indeed, according to literature, the mechanism of action of TTO relies on the denaturation of proteins, simultaneously altering the functions of bacteria cell membranes and walls, being highly effective against a wide variety of microorganisms [14,32]. On its turn, the strong antibacterial properties of CLO and CO result from one of their main elements, eugenol [10,13]. CLO presented slightly lower MBCs than CO. One possible explanation may be related to a larger eugenol content in CLO (Table S2 and S3 in Supporting Information). The antibacterial mechanism of action of CLO is often associated with its capacity to remain at the bacteria cell surface and, in parallel with this occurrence, altering the functions and structure of bacterium which finally results in the leakage of cell content [10]. On the other hand, CO mechanism relies on the disruption of the transports of ion and solutes in bacteria, passing through their membrane, leading to cell death [33].

Table 1
MBCs of the tested EOs against *S. aureus*, *S. epidermidis*, *E. coli* and *P. aeruginosa* reference strains.

EOs		*S. aureus*	*S. epidermidis*	*E. coli*	*P. aeruginosa*
CO	MIC (mg/mL)	2.060	2.060	3.500	39.300
	MBC (mg/mL)	4.125	4.125	8.250	>528.000
CLO	MIC (mg/mL)	2.050	0.830	1.024	52.800
	MBC (mg/mL)	4.100	1.024	1.024	>528.000
TTO	MIC (mg/mL)	1.748	1.748	1.748	3.500
	MBC (mg/mL)	3.500	1.748	1.748	3.500

In a general perspective, the three tested EOs showed lower MIC/MBC values towards the inhibition of Gram-positive bacteria than Gram-negative ones (only attending the tested lot of bacteria strains). Similar results have been previously reported, addressing the superior endurance of Gram-negative bacteria towards the action of the hydrophobic biomolecules present in EOs. According to Kamel et al., the lipid bilayer present in Such the Gram-negative bacteria, tends to offer higher protection to the bacteria cells, therefore limiting the passage of external invaders, including EO molecules [14,32].

3.2. Wet-spun fiber morphology

For a better understanding on the influence in rheological properties upon the presence of the three tested EOs, the viscosities of PCL, PCL-CO, PCL-CLO, PCL-TTO, CA and CA-PEG solutions were determined as a function of temperature (Fig. S1 in Supporting Information). PCL presented higher viscosity in comparison with CA solution, likely related to the fact that the former has a higher Mw. Furthermore, the addition of CLO resulted in a decrease in the viscosity of PCL solution.. Such result was also expected due to the high affinity between EOs and PCL and, therefore, influencing the rheological properties of the PCL solution [11,13]. Interestingly, as CO possesses a higher density in comparison with CLO and TTO, a higher viscosity for the PCL-CO solution was attained. Another decrease in viscosity was observed after the addition of PEG to the CA solution. Several reports address the formation of intermolecular hydrogen bonding of hydroxyl groups from CA with PEG, along with interactions of PEG hydroxyl groups with CA carbonyl groups [34,35]. Such interactions, together with the fact that PEG has a lower Mw than CA, justify the decrease of the solution viscosity.

SEM micrographs of the fibers' cross-section, morphology via brightfield microscopy, physical images of the fibers at macroscopic view and average diameters are shown in Fig. 1 and Fig. S2 in Supporting Information. Apart from TTO, incorporation of EOs into PCL fibers resulted in an increase of the core's thickness (e.g., 158.699 μm from PCL fibers to 201.554 μm from PCL-CLO fibers). One possibility for this outcome relies on the fact that, since both CO and CLO present higher affinity with PCL, alterations were introduced to the PCL polymeric chains, giving rise to less constricted structures in PCL-CO and PCL-CLO fibers [13,36]. That same observation was made by Unalan et al., in which the incorporation of CO onto PCL and gelatin electrospun nanofibers resulted in an increase in the fibers' diameters [37]. In fact, the high affinity between PCL and eugenol has already been demonstrated by the formation of intricate interactions between eugenol's hydroxyl groups and PCL's carbonyl groups [11].

On the other hand, since TTO does not contain eugenol, the opposite effect on the fibers' diameter was attained.

In general, the core's thickness within the coaxial fibers was superior to the thickness of monolayered fibers (e.g., core thickness of 280.933

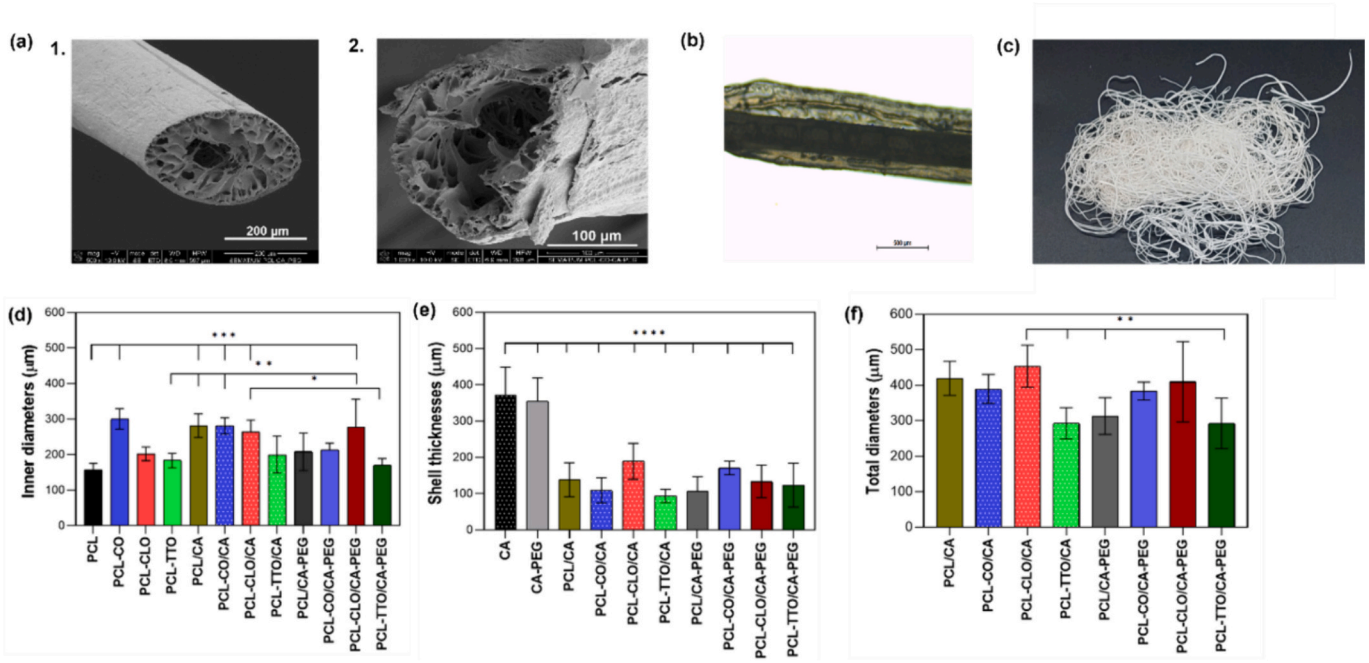

Fig. 1. Micrographs of the PCL-TTO/CA-PEG wet-spun fibers' morphology obtained by (a) SEM: 1. PCL/CA-PEG (272.00 ± 72.919 µm) (magnification of 500 x, 200 µm scale bar), 2. PCL-CO/CA-PEG (183.860 ± 25.221 µm) (magnification of 1000 x, 100 µm scale bar); (b) micrographs of CA-PEG wet-spun fibers' morphology obtained by brightfield microscopy and (c) images of PCL-CLO/CA fibers attained by macroscopic view: 1. single filament, 2. multi-filament. Distribution of (d) inner diameters (PCL as control), (e) shell thicknesses (CA and CA-PEG as controls) and (f) complete fiber diameters of all wet-spun fiber typologies (PCL/CA and PCL/CA-PEG as controls). Data are reported as mean ± SD ($n = 5$). Statistical significance was determined via Tukey test by applying multiple comparisons between the different fiber typologies (*$p < 0.0226$, **$p < 0.0078$, ***$p < 0.006$, ****$p < 0.0001$).

µm in PCL/CA fibers). This can be explained by the affinity between PCL and CA polymers, which were also dissolved in the same solvent. Consequently, interactions between the core and shell components occurred, along with the expansion of the inner layer by partially incorporating the shell (Fig. 1a and b). In fact, many reports have shown the successful blending of CA with PCL that establish interactions between hydroxyl groups present in CA polymeric chains together with carbonyl groups of PCL polymeric chains [38]. Coaxial fibers containing solely CA at the shell exhibited similar thickness ranges compared to the coaxial fibers with a shell made of CA and PEG (e.g., total diameter of 389.623 µm was achieved for PCL-CO/CA fibers and a diameter of 383.717 µm was attained for PCL-CO/CA-PEG fibers). This observation is expected considering both the PEG and the EOs were added to the fibers at very low proportions compared to the main polymers (CA and PCL). In the absence of the fibers' core, CA and CA-PEG hollow fibers presented larger shell thicknesses (e.g., 370.667 µm for CA fibers and 280.933 µm for PCL/CA fibers). A similar outcome was attained in a previous research from our team, in which hollow wet-spun fibers displayed higher thicknesses in comparison with shell thicknesses of coaxial fibers [39]. Such result is caused by a higher expansion of polymeric chains from CA and PEG polymers, since both compounds are not restricted by any innermost layer [36].

3.3. ATR-FTIR

ATR-FTIR spectra were collected for all wet-spun fibers (Fig. 2) and their characteristic peaks were identified (Table S4 in Supporting Information). Characteristic peaks of PCL were detected in all PCL-containing fibers, the first one at 1728 cm^{-1} and the second at 2950 cm^{-1} . According to literature, the former peak refers to PCL's carbonyl groups, whereas the latter is referent to C—H vibrations. Bands centered at 1166 and 1250 cm^{-1} were also detected, being associated with C-O-C vibrations [40]. On its turn, the presence of CA in all CA-containing fibers was proven by the peaks centered at 1738 and 1660 cm^{-1}, linked to the polymer carbonyl and possible H-O-H bending of absorbed water, respectively [41]. Moreover, peaks referring to the CH_2 vibrations, acetyl ester groups and C—O stretching vibrations were detected at 1438, 1222 and 1044 cm^{-1}, respectively [42]. The occurrence of PEG was confirmed on all PEG-containing fibers by a more intense peak centered at 3310 cm^{-1} (due to OH stretching vibrations) and through a shift of the carbonyl peak from 1738 to 1732 cm^{-1}. According to Majumder et al., the former happens due to the formation of intermolecular hydrogen bonding between CA and PEG [34]. Whereas, according to Chen et al., the latter results from the interactions of the hydroxyl groups of PEG with the carbonyl groups of CA [35]. Since CO, CLO and TTO were loaded into the fibers at low concentrations (high polymer/EOs content ratio), it was not possible to confirm their presence with the present technique.

3.4. Differential scanning calorimetry

The thermal behaviors of all wet-spun fibers were assessed by DSC thermograms (Fig. 3) and the main characteristic peaks were identified (Table S5 in Supporting Information).

The presence of PCL was detected by a first endothermic peak, perceived in the PCL fibers (Fig. 3a),centered at 59.24 °C (onset at 52.85 °C and endset at 63.78 °C), translating into the melting point of the polymer. Another highly pronounced peak was then observed at ≈ 422.37 °C (onset at 413.17 °C and endset at 448.16 °C) which represents the complete degradation of PCL [43]. The effect of the incorporation of EOs onto PCL fibers was also detected, resulting in small shifts in PCL melting temperatures (e.g., from 59.24 °C to 56.89 °C in relation to PCL-CLO fibers), along with an increase in the enthalpy (e.g., from −327.94 mJ to −243.16 mJ, again for PCL-CLO fibers). According to Zhelyazkov et al., EOs are endowed with a plasticizing effect that leads to higher chain mobility, explaining the present results [44]. Another relevant factor which justifies these occurrences consists in the good miscibility between both PCL and EOs, generally resulting in small shifts of

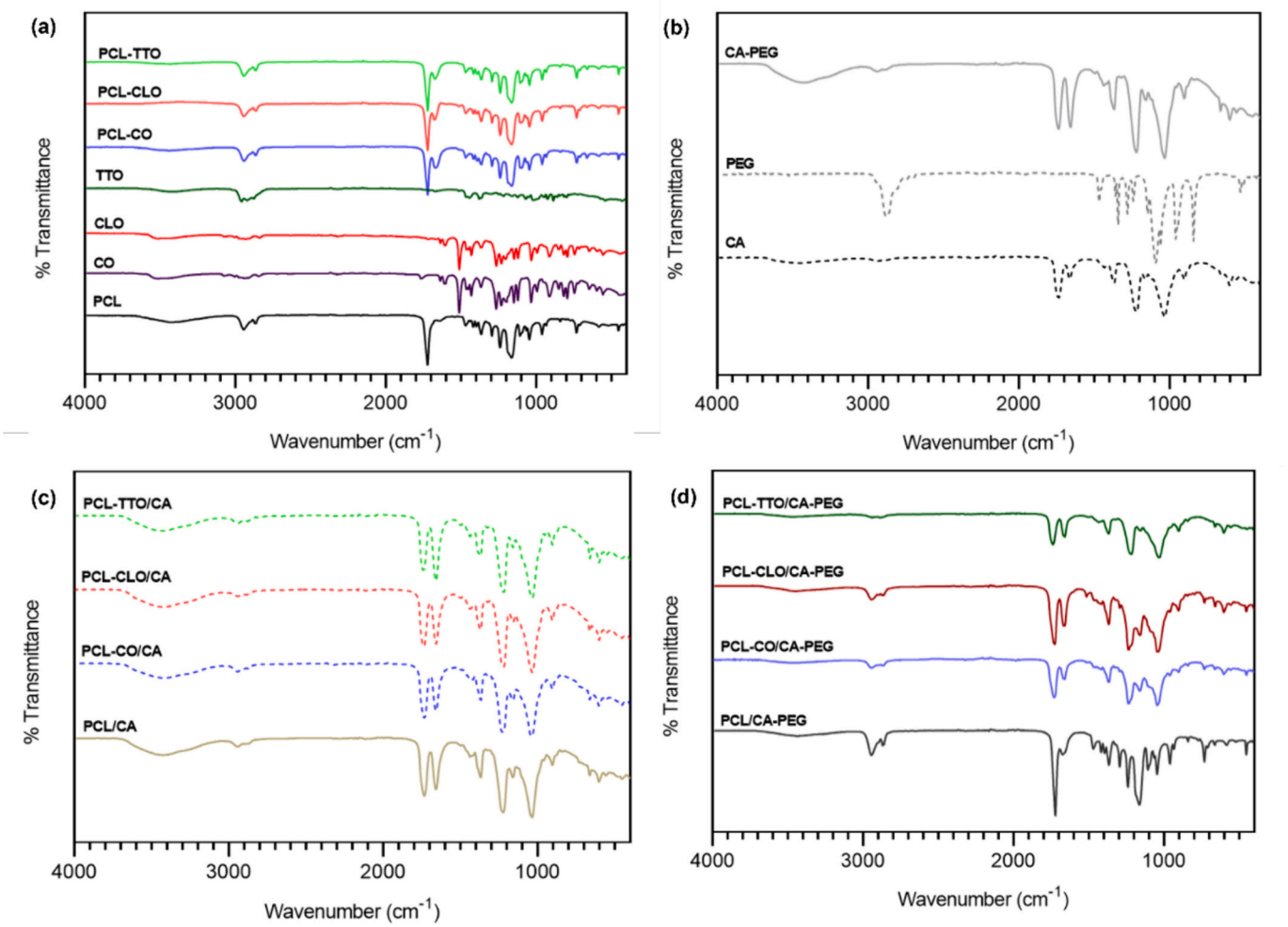

Fig. 2. ATR-FTIR spectra of (a) CO, CLO and TTO (liquid form); PCL, PCL-CO, PCL-CLO and PCL-TTO fibers; (b) PEG powder, CA and CA-PEG fibers; (c) PCL/CA, PCL-CO/CA, PCL-CLO/CA and PCL-TTO/CA coaxial fibers; and (d) PCL/CA-PEG, PCL-CO/CA-PEG, PCL-CLO/CA-PEG and PCL-TTO/CA-PEG coaxial wet-spun fibers.

endothermic peaks [45]. On the other hand, PCL-TTO fibers showed a lower melting temperature (≈ 45.32 °C) along with a higher enthalpy (−180.12 mJ) in comparison with CO/CLO-loaded fibers, which indicate, once more, that the interactions between this EO and PCL polymeric chains occurred less effectively. Once again, the different composition of TTO may be behind the observations (Table S1 in Supporting Information) [13].

On the other hand, CA fibers presented an endothermic peak centered at 93.46 °C (onset at 51.59 °C and endset at 118.51 °C) (Fig. 3b). According to Ribeiro et al., peaks centered at ≈ 100 °C are associated with the outflow of water molecules [46]. Another peak detected at ≈ 160.95 °C (onset at 128.34 °C and endset at 204.11 °C) was linked to the glass transition temperature of CA [46,47]. Finally, a third peak was detected at ≈ 223.45 °C (onset at 215.29 °C and endset at 228.74 °C), ascribed to the crystallization of the amorphous domains of the CA chains [46]. The addition of PEG to the CA fibers resulted in the appearance of a peak at ≈ 36.73 °C (onset at 28.23 °C and endset at 41.37 °C), which is attributed to the exothermic crystallization of PEG [35]. A peak at ≈ 88.63 °C (onset at 54.59 °C and endset at 112.85 °C) was also observed as a result of the interactions between CA and PEG that shifted the peak detected in the pristine CA fibers at 93 °C. Additionally, the melting endothermic peak of PEG was shifted since, according to Chen et al., that peak usually occurs in the range of 50–70 °C. Considering interactions between hydroxyl groups in PEG and carbonyl groups in CA are frequent, this justifies the shift from the characteristic peak of PEG [35]. Finally, the characteristic endothermic peak of CA observed at ≈ 223.45 °C was maintained and another endothermic peak related to the pyrolysis process of PEG appeared at ≈ 368.23 °C (onset at 217.30 °C and endset at 377.09 °C), which frequently occurs around 350 °C [48]. According to Faradilla et al., the temperature of its pyrolysis process is directly proportional to the Mw of PEG, explaining the augment in ≈ 18 °C compared to the literature [48].

The characteristic PCL, CA and PEG peaks were also observed in the coaxial fibers. Similarly to the monolayered fibers, the addition of EOs resulted in small shifts in the PCL characteristic peaks and in a reduction of enthalpy, which is also in accordance with the results from Fig. 3a. PCL/CA-PEG fibers displayed a peak centered at 46.25 °C (onset at 41.02 °C and endset at 49.17 °C), which was originated from the crystallization exothermic peak of PEG, detected at 36 °C in the CA-PEG fibers [49], combined with the melting point of PCL, detected at 55 °C in the PCL fibers [43]. Additionally, a peak centered at 90.93 °C (onset at 63.35 °C and endset at 113.79 °C) was registered, ascribed to the outflow of water molecules from CA. At 148.20 °C (onset at 128.51 °C and endset at 162.34 °C), a different peak was also detected corresponding to the glass transition temperature of CA [46].

3.5. Thermogravimetric analyses

Thermogravimetric analyses (TGA) analyses allow the determination of the degradation temperature from each fiber component, relevant to detect the capacity for the proposed system to undergo several sterilization processes, while keeping its structure intact when exposed to

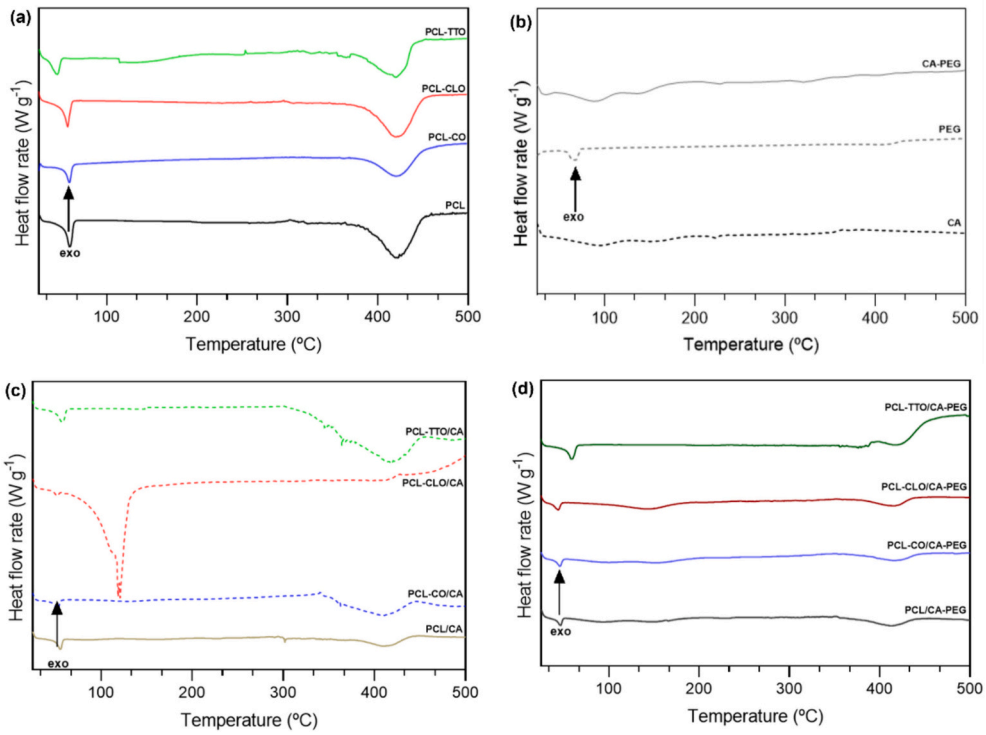

Fig. 3. DSC thermograms of (a) PCL, PCL-CO, PCL-CLO and PCL-TTO fibers, (b) CA and CA-PEG hollow fibers, (c) PCL/CA, PCL-CO/CA, PCL-CLO/CA and PCL-TTO/CA coaxial fibers and (d) PCL/CA-PEG, PCL-CO/CA-PEG, PCL-CLO/CA-PEG and PCL-TTO/CA-PEG coaxial wet-spun fibers (complete form).

body temperatures [50]. Furthermore, levels of retention from such samples can also be analyzed, determining the ability of the system to maintain a moist wound environment, essential for accelerating the wound healing process [51]. It is also relevant to mention that, with this technique, it is possible to compare thermograms of individual polymers with composite samples, this way detecting if any chemical interaction was established between the tested materials. As a result, TGA determinations were performed to uncover the wet-spun fibers degradation steps (Fig. 4).

PCL monolayer fibers registered high mass losses only at temperatures superior to 350 °C, as evidenced in the respective DTG curve (Fig. 4e) and coherent with the endothermic peak detected at 422.37 °C by DSC (Fig. 3a) [52]. The incorporation of EOs onto PCL fibers lowered the degradation temperatures (to ≈ 270 °C). According to Phaiju et al., when EOs are successfully incorporated into a polymeric matrix, they influence the polymeric chains orientation and decrease the crystallinity of the structure, explaining earlier degradations [45].. Still, CO and CLO-loaded fibers endured slightly smaller mass losses occurring at slower rates than TTO-containing fibers, highlighting the effective thermal stability of the structures and confirming that a strong network was generated with PCL. On its turn, TTO-loaded fibers suffered higher mass losses that occurred at a faster rate. Such result is associated with the smaller fiber diameters, resulting from lower intermolecular bonds with PCL [11,13], which compromised the fibers' thermal stability (as evidenced in the DSC data, Fig. 3).

CA fibers (Fig. 4b) endured small mass losses (≈ 5 %) up until 200 °C related with water molecule bonding with the hydroxyl groups of CA, as well as the deacetylation of CA. However, from 300 to 400 °C, CA fibers lost ≈ 75 % of their mass, representing the main thermal decomposing step of CA, as it is evidenced with a peak centered at ≈ 350 °C in the DTG thermogram (Fig. 4f), in which breakdown of glycosidic bonds occurred. Finally, at temperatures superior to 400 °C, CA fibers lost their remaining mass at a slower rate, corresponding to the fibers' complete degradation and decomposition [53]. Interestingly, on its own, PEG started suffering mass reductions at a higher temperature (≈ 355 °C). This observation is in accordance with several reports that show the pyrolysis process of PEGs with molecular weights higher than 1000 Da to occur around 300/350 °C. In addition, its thermal decomposition usually takes place between 340 °C and 415 °C, also shown in the respective DTG representation, and is predicted to start at the -C-O- and -C-C- bonds of its backbone chains [48,54]. On its turn, CA-PEG fibers experienced lower thermal stability at 200 °C and higher mass losses compared to CA alone, between 300 and 400 °C, corroborating DSC data (Fig. 3b) [55].

PCL/CA fibers reported thermal stability until ≈ 250 °C, after which they lost near 73 % of their mass (300–400 °C), presenting a first peak shown in their DTG curve (Fig. 4g). Additionally, such fibers reached almost complete degradation at ≈ 450 °C (second peak present in DTG thermogram) [52,53]. Data was consistent with the observations made on the monolayered fibers and, in general, EOs incorporation onto coaxial fibers resulted in lower thermal stabilities (higher mass losses). On the other hand, PCL/CA-PEG fibers suffered higher mass losses until 200 °C and started degrading at a lower temperature (≈ 250 °C) compared with the PCL/CA fibers. The differences in the thermal behavior were caused by the interactions established between CA and PEG, which altered the polymeric chains and crystallinity of CA [55]. Such observation is coherent with the thermal peaks attained at 148 °C and 223 °C in the DSC spectra of coaxial fibers, referring to CA glass transition temperature (Fig. 4c).

3.6. Mechanical testing

The mechanical properties of the wet-spun fibers were evaluated by their maximum elongations at break and breaking strengths (Table 2). CA and CA-PEG hollow fibers could not be analyzed due to their rigid nature (reduced elasticity) and paper-like consistency [56]. On its turn, all the remainder engineered wet-spun fibers showed elongations at break superior to 300 %, along with breaking strengths of over 8 kPa, resulting from the presence of PCL, which high elasticity has been disclosed in several reports. [57]. Apart from the PCL-TTO combination, all

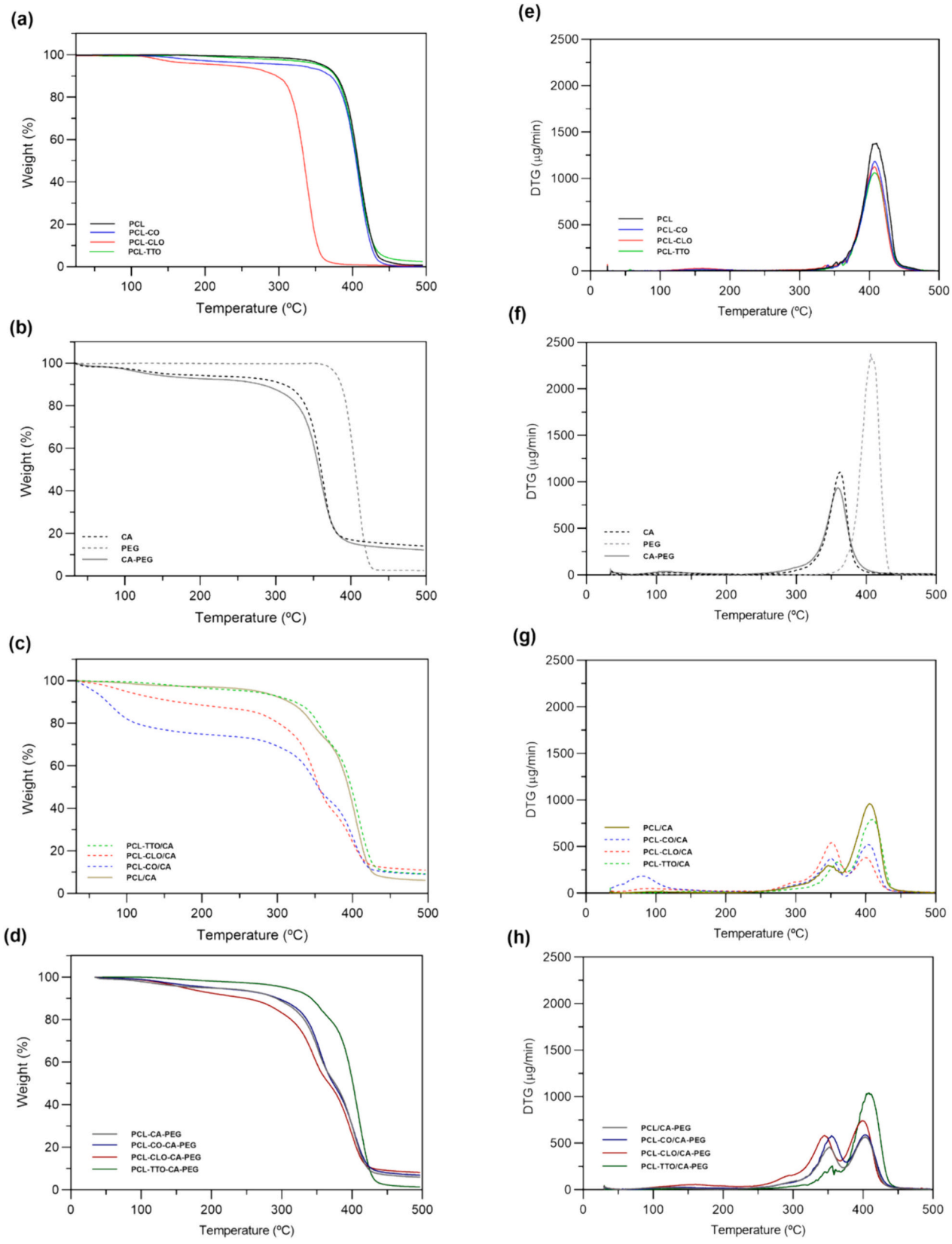

Fig. 4. TGA thermograms of (a) PCL, PCL-CO, PCL-CLO and PCL-TTO fibers and (e) respective DTG curves, (b) CA and CA-PEG hollow fibers and (f) respective DTG curves, (c) PCL/CA, PCL-CO/CA, PCL-CLO/CA and PCL-TTO/CA coaxial fibers and (g) respective DTG curves, (d) PCL/CA-PEG, PCL-CO/CA-PEG, PCL-CLO/CA-PEG and PCL-TTO/CA-PEG and (h) respective DTG curves, coaxial wet-spun fibers (complete form).

Table 2
Mechanical examinations of the engineered wet-spun fibers. Data is reported as mean ± SD ($n = 4$).

Fiber typology	Maximum elongations at break (%)	Breaking strength (kPa)
PCL	337.50 ± 34.26	8.21 ± 1.18
PCL-CO	338.95 ± 28.58	11.89 ± 0.78
PCL-CLO	342.32 ± 20.12	17.55 ± 5.45
PCL-TTO	323.62 ± 36.92	17.55 ± 8.41
PCL/CA	358.97 ± 14.69	17.27 ± 8.09
PCL/CA-PEG	333.02 ± 32.50	15.29 ± 5.04
PCL-CO/CA	343.52 ± 30.97	85.63 ± 1.55
PCL-CLO/CA	341.78 ± 1.30	13.02 ± 3.07
PCL-TTO/CA	315.21 ± 67.64	9.62 ± 1.93
PCL-CO/CA-PEG	360.16 ± 0.36	11.75 ± 0.88
PCL-CLO/CA-PEG	349.61 ± 17.32	10.62 ± 0.75
PCL-TTO/CA-PEG	328.08 ± 35.79	9.70 ± 2.60

monolayered fibers presented similar maximum elongations at break (no significant differences were found, Table S6 in Supporting Information) showing that the addition of EOs does not significantly alter the fibers' mechanical performance. Such observations were expected since EOs were loaded at low concentrations and are frequently used as plasticizers for improving the physical and mechanical properties of several structures [58]. The reduced affinity between TTO and PCL alsoimpacted on the mechanical stability of the fibers most likely due to the disorganization of the structure and the smaller number of interactions established between the two compounds [11].

Regarding coaxial fibers, the shell successfully functioned as a barrier and prolonged the rupture of the fibers' core, generating the highest maximum elongations at break (Fig. S3 in Supporting Information) [59]. Coaxial fibers made with a shell of CA displayed slightly lower mechanical resilience compared to coaxial fibers with a shell of CA and PEG. This can be explained by the intermolecular hydrogen bonding between CA and PEG, along with interactions between hydroxyl groups in PEG and carbonyl groups in CA, forming a compact structure [34,35]. Once more, TTO-loaded coaxial fibers presented lower maximum elongations at break. Nevertheless, such results are still within acceptable values for their envisioned application.

3.7. Swelling capacity

The degree of swelling for all wet-spun fibers was assessed by measuring mass alterations after incubation in PBS at 37 °C (pH 7.4) until saturation was reached, which was observed at day 7 (Fig. 5 and Table S7 in Supporting Information). In general, mass variations decreased with the prolonged exposure to the medium. Li et al. reached similar outcomes while examining the swelling index of core-shell structures. They concluded this to be an effect of the polymeric erosion experienced by both layers [60]. The PCL's hydrophobic nature combined with the also hydrophobic EOs significantly reduced the fibers ability to interact with the surrounding water molecules [61]. Moreover, the addition of EOs interfered with the interactions of the PCL chains with PBS salts, reducing even more the degree of swelling of the fibers compared to the pristine PCL [44]. Literature reports on CO-loaded structures confirmed these findings by registering lower hydration properties in comparison to the EO-unloaded samples (control) [15,60]. To the contrary, CA and CA-PEG hollow fibers reached the highest swelling ratios, once more due to the higher freedom for interactions between medium and CA polymeric chains, caused by the absence of the innermost layer (i.e., PCL). Also, the swelling capacity of CA is related with the spacing between its polymeric chains, which limits the intermolecular attraction forces and increases chain mobility, thus resulting in the retention of more PBS molecules [62]. Remarkably, all coaxial fibers attained the smallest degrees of swelling, which decreased even further upon the addition of PEG. Even though PEG is a hydrophilic

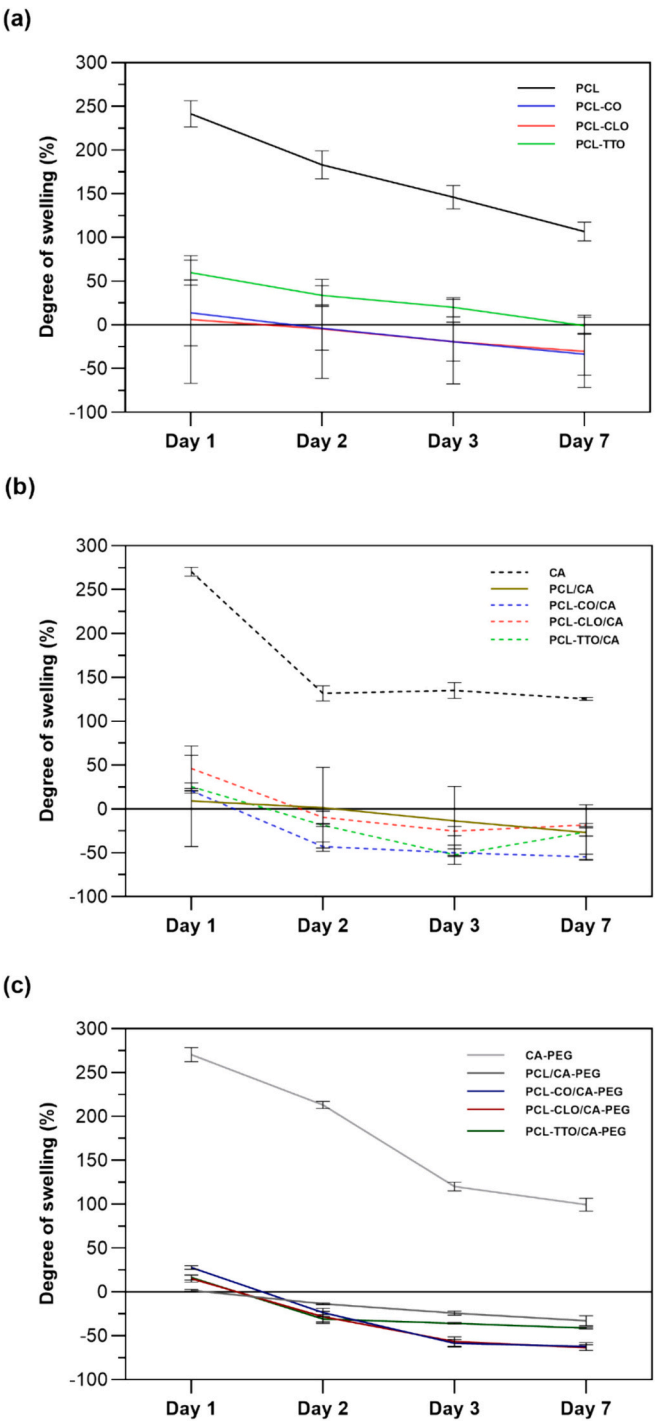

Fig. 5. Degrees of swelling overtime of (a) PCL, PCL-CO, PCL-CLO, PCL-TTO; (b) CA, PCL/CA, PCL-CO/CA, PCL-CLO/CA, PCL-TTO/CA; (c) CA-PEG; PCL/CA-PEG; PCL-CO/CA-PEG, PCL-CLO/CA-PEG, PCL-TTO/CA-PEG wet-spun fibers over 7 days of incubation in PBS. Data is presented as average percentage of degree of swelling (D.S.) ± SD ($n = 3$).

polymer, it is likely this polymer to have blocked the water molecules access to the CA and PCL polymer chains by interacting with these polymers through the same sites [63]. Indeed, most hydroxyl groups of PEG interact strongly with the carbonyl or hydroxyl groups of CA, generating a dense structure (as evidenced by the mechanical properties of the fibers), which may limit the interfaces with the surrounding medium [35]. Similarly to the monolayered fibers, the loading of EOs decreased the swelling properties of PCL/CA and PCL/CA-PEG samples.

3.8. Degradation profile

The stability of EOs-loaded and unloaded wet-spun fibers in physiological media was evaluated by the fibers' incubation in PBS up to 28 days at 37 °C (pH 7.4). The degradation of the fibers was visually evaluated and the mass changes over time were registered for each fiber typology (Fig. 6, Table S8 and Fig. S4 in Supporting Information).

CA and CA-PEG hollow fibers presented smaller mass losses during the initial 7 days of incubation, likely due to the presence of CA, which strong mechanical stability has been reported in literature [26]. Nevertheless, as PEG is a hydrophilic compound, it is possible that this factor contributed to a faster dissolution of polymer fragments into PBS media, resulting in higher mass losses from CA-PEG fibers in the following days of incubation [64]. Still, both fiber typologies maintained their structures, proving the mechanical stability of CA [26]. All remaining fibers preserved their structural integrity throughout the 28 days of incubation, due to the high mechanical performances of PCL [65].

Monolayer fibers reported higher stabilities (lower mass losses) in comparison with the coaxial fibers. This was expected since the absence of shell components resulted in higher freedom of the PCL polymeric chains and, thus, potential breakable sites originated from the interactions with the shell polymers could be avoided, maintaining the stability of the fibers. The addition of EOs onto the monolayer fibers led to a slightly higher mass variation during the initial 7 days of incubation in PBS. Afterwards, mass reductions were less important. EOs can alter the organization of the PCL polymeric chains, consequently changing the steadiness of the structures. Also, the high volatility of EOs translated into their likely total evaporation after the initial 7 days of incubation, not compromising the stability of the fibers throughout the remaining days of incubation in PBS [11].

On its turn, the EO-loaded coaxial fibers registered slightly lower mass variations compared with the coaxial EO-unloaded fibers, possibly due to the presence of the shell components which interfered with the interactions between EO molecules and PCL polymeric chains, resulting in a smaller influence on the stability of PCL [18,19]. In addition, although all coaxial fibers remained stable during the entire period of incubation in PBS, the fibers which shell contained solely CA presented slightly lower mass variations in comparison with the remaining coaxial fibers. Such behavior can be explained by the presence of PEG, which, as shown earlier, represents a hydrophilic polymer that, not only can alter the conformation of CA but also can be dissolved in the media [66]. In summary, the unloaded and EO-loaded wet-spun fibers maintained their structure during the 28 days of incubation in PBS, proving their adequate stability for wound healing applications.

3.9. EOs release kinetics

The release kinetics of CO, CLO and TTO was mapped after 1, 2, 4, 6 and 24 h of incubation from all wet-spun fibers in PBS at 37 °C and pH 7.4 (Fig. 7). Cumulative release profiles of the three EOs were determined by comparison with the calibration curves of the analyzed EOs (Fig. S5 in Supporting Information). EOs-unloaded fibers were also analyzed, this way subtracting the polymers' influence from the results of EO-loaded fibers. No significant changes were detected on the morphology of CLO-loaded fibers throughout the 24 h of fibers incubation in PBS (Fig. S6 in Supporting Information).

The absence of shell components, which usually display a protective effect, led to higher EOs release rates from monolayer fibers in comparison to the coaxial fibers. Similar remarks were made with the release of CO from gellan gum bilayer films compared to the monolayered samples [60].

CLO-containing fibers experienced the highest release kinetics, particularly during the first 6 h of the test. After this point, lower rates were registered, which is consistent with data acquired from CLO-loaded core-sheath nanofibers and hydrogels by Jung et al. [67]. As the initial burst release occurs, the quantity of EO present on the fibers reduced, thus decreasing its release rate after 6 h of incubation (the peak). A slightly higher EO release was detected for the PCL-CLO/CA-PEG fibers compared to the PCL-CLO/CA. It appears that the shell protection in physiological-like media is reduced in the presence of PEG, leading to higher release rate of CLO. The hydrophilicity of PEG led to a faster dissolution onto the media, resulting in the degradation of the shell from PCL-CLO/CA-PEG fibers (Fig. 6) [63].

In addition, CO followed a similar release profile in comparison with fibers' degradation in PBS (Fig. 6). Between the three tested oils, TTO-loaded monolayer and coaxial fibers reported the smallest releases. Here, the lack of affinity between polymer and oil reduced TTO entrapment (smaller fiber diameters, Fig. 1), being some of the weakly bound oil molecules washed away in the coagulation bath during fiber production.

3.10. Antioxidant activity

DPPH radical scavenging activity assay was applied to evaluate the antioxidant activity of EO-loaded fibers. Samples were immersed in absolute ethanol during 1, 2, 4, 6 and 24 h and their antioxidant properties were monitored continuously during 1 h (Fig. 8). Such property is crucial for wound healing since, during the inflammatory phase, biologically active mediators will attract neutrophils, leukocytes and monocytes to the wound site, leading to a significant increase in free radicals. When those radicals reach excessive levels, the cell oxidant and antioxidant equilibrium is altered, enzymes are inactivated, DNA is damaged and lipid peroxidation occurs, all delaying the wound healing process. Therefore, wound healing can be enhanced by the introduction of antioxidant compounds capable of reducing the presence of free radicals surrounding wound sites [33].

The incubation period did not significantly influence the fibers' antioxidant activities. The strong antioxidant activities of both CO and CLO resulted from the presence of eugenol [29]. Yet, CLO was more effective than CO. This occurs because CO possesses other components in its composition besides eugenol, namely eugenyl acetate and beta-caryophyllene, which antioxidant profile is not as important as eugenol [37]. In addition, CLO presented higher release profiles in comparison to CO and TTO (Fig. 7), allowing for a greater availability and facilitated access to the oil. On the other hand, TTO's antioxidant properties, linked not only to the component terpinene-4-ol but also to the 4-methyl-1-(1-methylethyl)bicyclo[3.1.0]hexane didehydro derivative, an agent known to decrease oxidative stress, were not as important [68]. Its low release kinetics associated with a smaller amount on the fibers due to the lack of affinity with PCL can explain the reduced antioxidant activity [32].

EO-loaded monolayer fibers showed greater antioxidant activities compared to the coaxial, since in the absence of the shell the protective barrier function is lost and little restrictions are in place for accessing the EOs, which also resulted in higher release rates for the monolayer fibers. Interestingly, differences in the activities between CA and CA-PEG coaxial fibers have also been detected. CA coaxial fibers have shown lower antioxidant activities, related with the more sustained release profiles of the three EOs from the fibers.

Generally, data demonstrated that the EOs, particularly the CO and CLO, interfere with hydrogen peroxide-induced free radicals, augmenting cell protection against oxidative stress. Thus, confirming the fibers' potential to accelerate and enhance the wound healing process [33].

3.11. Bacteria inhibition

The antibacterial properties of all wet-spun fibers against *S. aureus*, *S. epidermidis*, *E. coli* and *P. aeruginosa* were tested by fibers' incubation in MHB at 37 °C up to 24 h. Results are expressed in % of inhibition of the four bacteria activities (Fig. 9 and Table S9 in Supporting

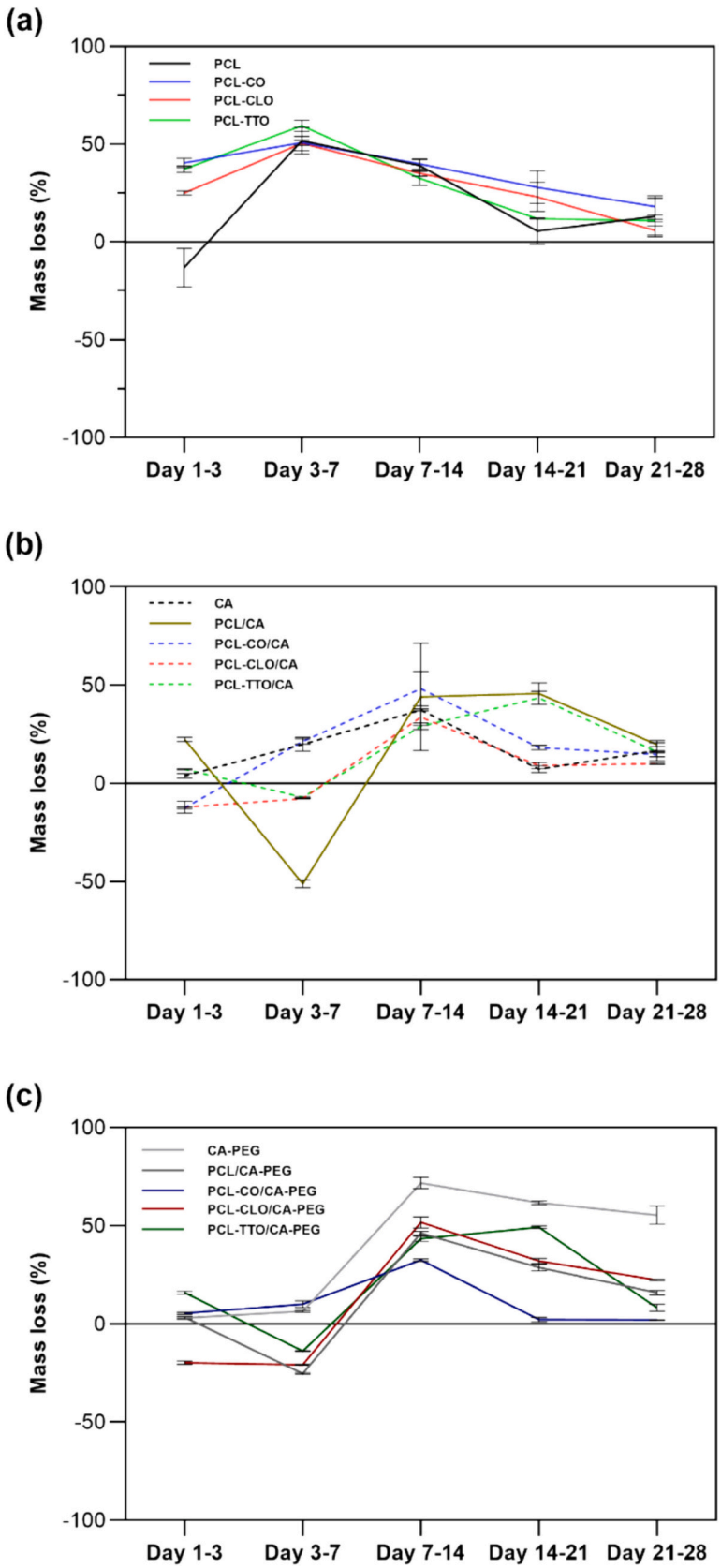

Fig. 6. Degradation profiles throughout 28 days of incubation in physiological-like media from (a) PCL, PCL-CO, PCL-CLO and PCL-TTO; (b) CA, PCL/CA, PCL-CO/CA, PCL-CLO/CA and PCL-TTO/CA; (c) CA-PEG, PCL/CA-PEG, PCL-CO/CA-PEG, PCL-CLO/CA-PEG and PCL-TTO/CA-PEG wet-spun fibers over 28 days of incubation in PBS. Data is presented as average percentage of mass loss ± SD ($n = 3$).

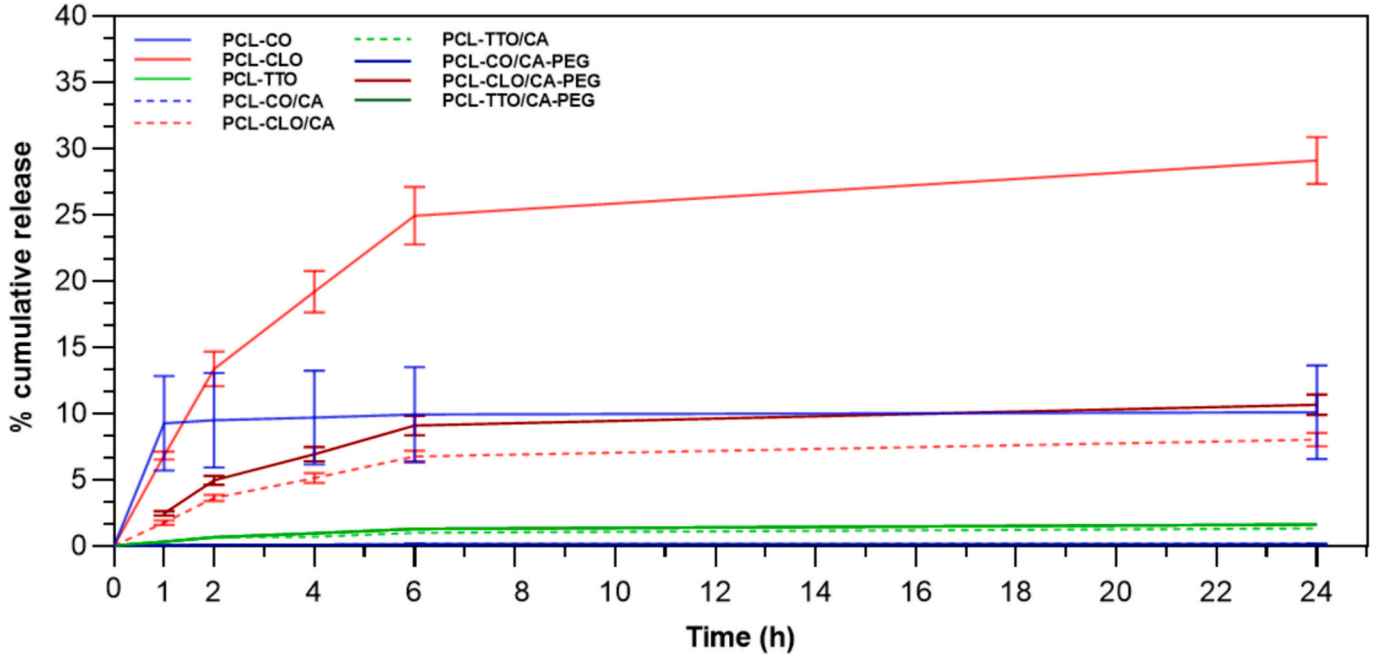

Fig. 7. Cumulative release profile of EO-loaded wet-spun fibers. Data are reported as mean ± SD ($n = 3$). Statistical significance was determined via Tukey test, applying multiple comparisons between the different fiber typologies (significance between PCL-CO and PCL-CLO, PCL-TTO, PCL-CLO/CA, PCL-TTO/CA, PCL-CO/CA-PEG, PCL-TTO/CA-PEG: $p < 0.0001$; significance between PCL-CLO and PCL-TTO, PCL-CO/CA, PCL-CLO/CA, PCL-TTO/CA and PCL-CO/CA-PEG, PCL-CLO/CA-PEG and PCL-TTO/CA-PEG: $p < 0.0001$; significance between PCL-CO/CA and PCL-CLO/CA, PCL-TTO/CA, PCL-CO/CA-PEG, PCL-CLO/CA-PEG and PCL-TTO/CA-PEG: $p < 0.0001$; significance between PCL-CLO/CA and PCL-TTO/CA, PCL-CO/CA-PEG, PCL-CLO/CA-PEG and PCL-TTO/CA-PEG: $p < 0.0001$; significance between PCL-TTO/CA and PCL-CO/CA-PEG, PCL-CLO/CA-PEG and PCL-TTO/CA-PEG: $p < 0.0001$, PCL-CO/CA-PEG and PCL-CLO/CA-PEG, PCL-TTO/CA-PEG: $p < 0.0001$; and significance between PCL-CLO/CA-PEG and PCL-TTO/CA-PEG: $p < 0.0001$). Data from EOs-unloaded fibers was subtracted to all EO-loaded fibers so the polymers' interference could be eliminated from the results.

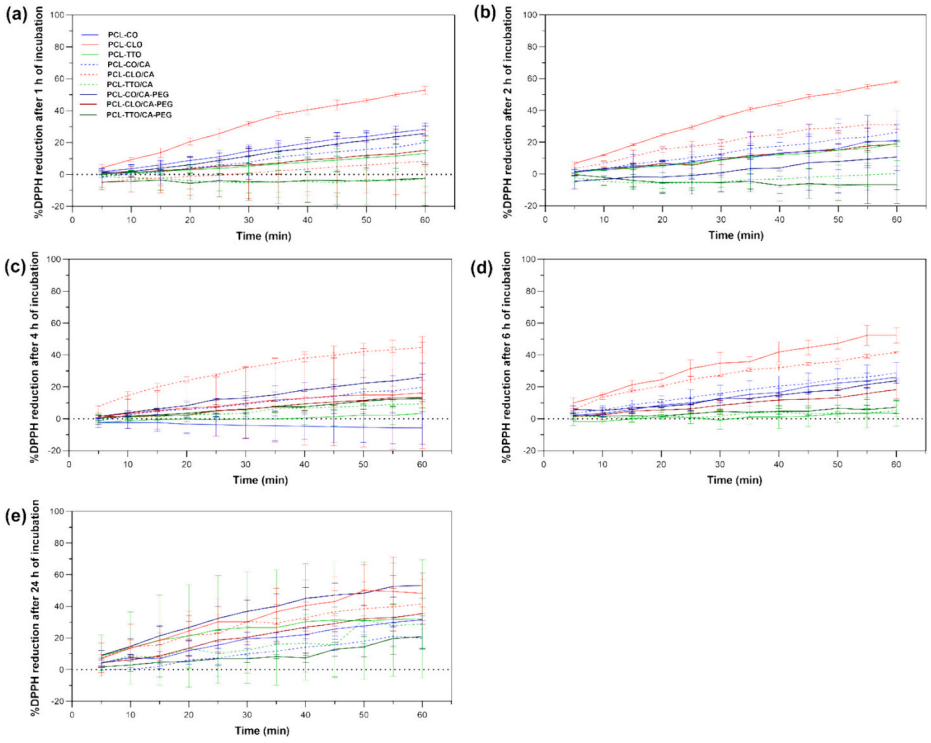

Fig. 8. DPPH reduction induced by EO-loaded wet-spun fibers after (a) 1, (b) 2, (c) 4, (d) 6 and (e) 24 h of incubation. Data are reported as mean ± SD ($n = 3$). Statistical significance was determined via Tukey test, applying multiple comparisons between the different fiber typologies; no statistical significance was found between fiber typologies.

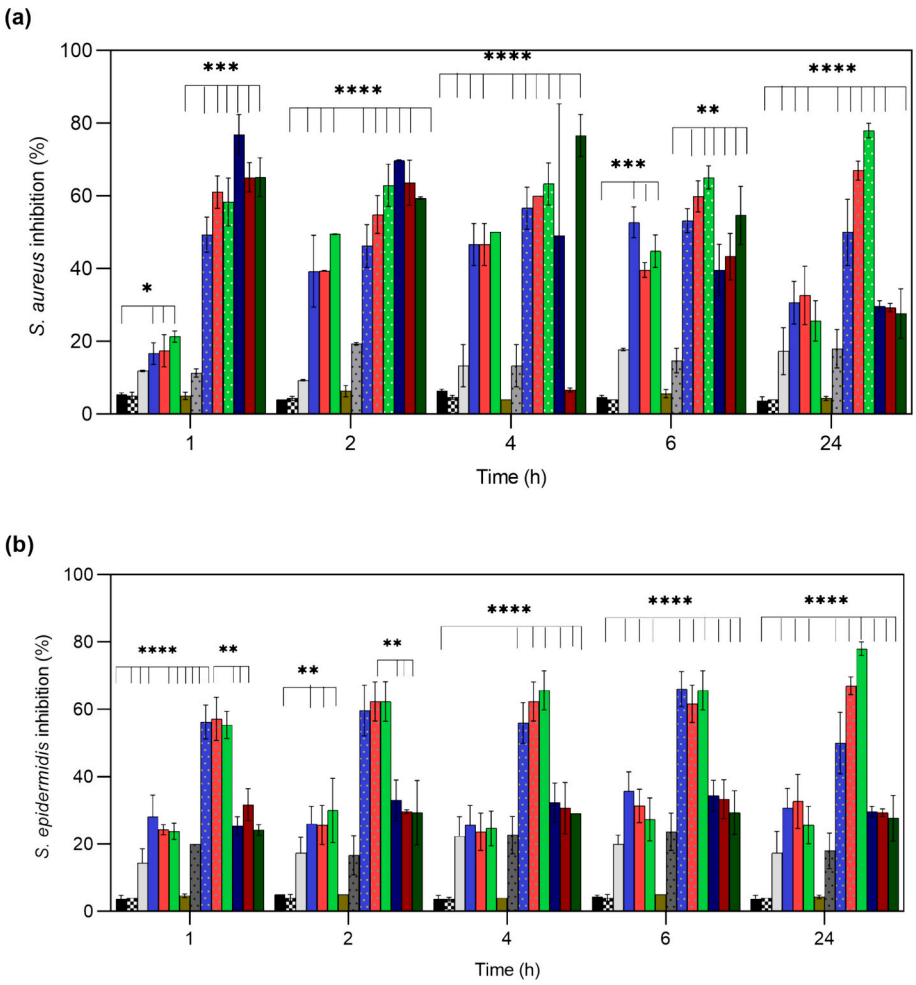

Fig. 9. Inhibitions of (a) *S. aureus*, (b) *S. epidermidis*, (c) *E. coli* and (d) *P. aeruginosa* bacteria in contact with all wet-spun fibers incubated in PBS for 1, 2, 4, 6 and 24 h.Data are reported as mean ± SD ($n = 3$). Statistical significance was determined via Tukey test applying multiple comparisons between the different fiber typologies $^{*}p < 0.05$; $^{**}p < 0.01$; $^{***}p < 0.001$ and $^{****}p < 0.0001$.

Information). EO-unloaded fibers presented residual antibacterial effect, possibly due to the fibers' porosity (Fig. 1). CA-PEG and PCL/CA-PEG fibers inhibited bacterial growth due to the PEG's antibacterial profile. Still, their effect was not significant considering the low proportion in which PEG was present in the fibers.

EOs-loaded fibers were the most antibacterial from the group. These observations were expected since strong antibacterial properties have been associated with the CO, CLO and TTO oils [15,33]. The EOs antibacterial effects are a result of their capacity to disrupt processes related with the transport of ions and solutes through the bacteria cell membrane. In fact, it is the EOs lipohilicity that enables their passage through the bacteria membrane, followed by their attack to intracellular components and ultimately resulting in cell death. In this case, the phenolic compounds are able to permeate the bacteria cell walls, block energy-producing enzymes and denature proteins present in the cell wall, damaging their barrier effect [33]. Many reports suggest the strong antibacterial properties of TTO originate from terpinenen-4-ol, along with 1,2,3,5-tetramethylbenzene (Table S1 in Supporting Information) [69]. Although the antibacterial mechanisms of action from the latter component are not reported in literature, studies have addressed its contribution to different EOs' antibacterial properties [31,69]. Regardless, terpinenenen-4-ol's mechanism relies on its ability to denature proteins and, simultaneously, change the structures and functions of cell membranes and walls [14,32]. On its turn, the antibacterial efficiency of both CO and CLO are linked to eugenol, one of their main components, which, in the case of CO, hinders ions and solutes transport and permeates the bacteria membrane [33]. On the other hand, CLO mechanism of action is associated with the disruption of cytoplasmic membrane's functions and integrities, caused by the ability of this EO to accumulate at the bacteria cell surface [10].

During the first 4 h of incubation, coaxial fibers, containing CA and PEG in the shell, presented higher antibacterial activity than coaxial fibers containing solely CA. Such observation may be justified with the faster release of the entrapped EOs (Fig. 7), most likely caused by the degradation of the CA-PEG shell, which factor also increased the fibers antioxidant activities (Fig. 8). After this point and considering that a large amount of the EOs had already been released from the CA-PEG coaxial fibers, the fibers' antibacterial effects reduced as time progressed. The present results are also in accordance with the fibers' evolution of antioxidant properties (Fig. 8), with DPPH reduction being stabilized after the 6 h mark. As CA shell experienced a slower degradation at the early stages of incubation than CA-PEG, thus inducing a more controlled and sustained release of the EOs, higher antibacterial effects were observed after the 4 h mark.

Generally, *S. aureus* experienced a higher reduction in activity than *S. epidermidis* (for example, 76.77 % vs 29.33 %, respectively, for PCL-CO-CA-PEG fibers), which could be easily explained by the lower efficacy of the selected EOs towards inhibiting *S. epidermidis.* In fact, several researches on EO-loaded structures have reported the antibacterial properties of CO, CLO and TTO towards *S. aureus*, *E. coli* and

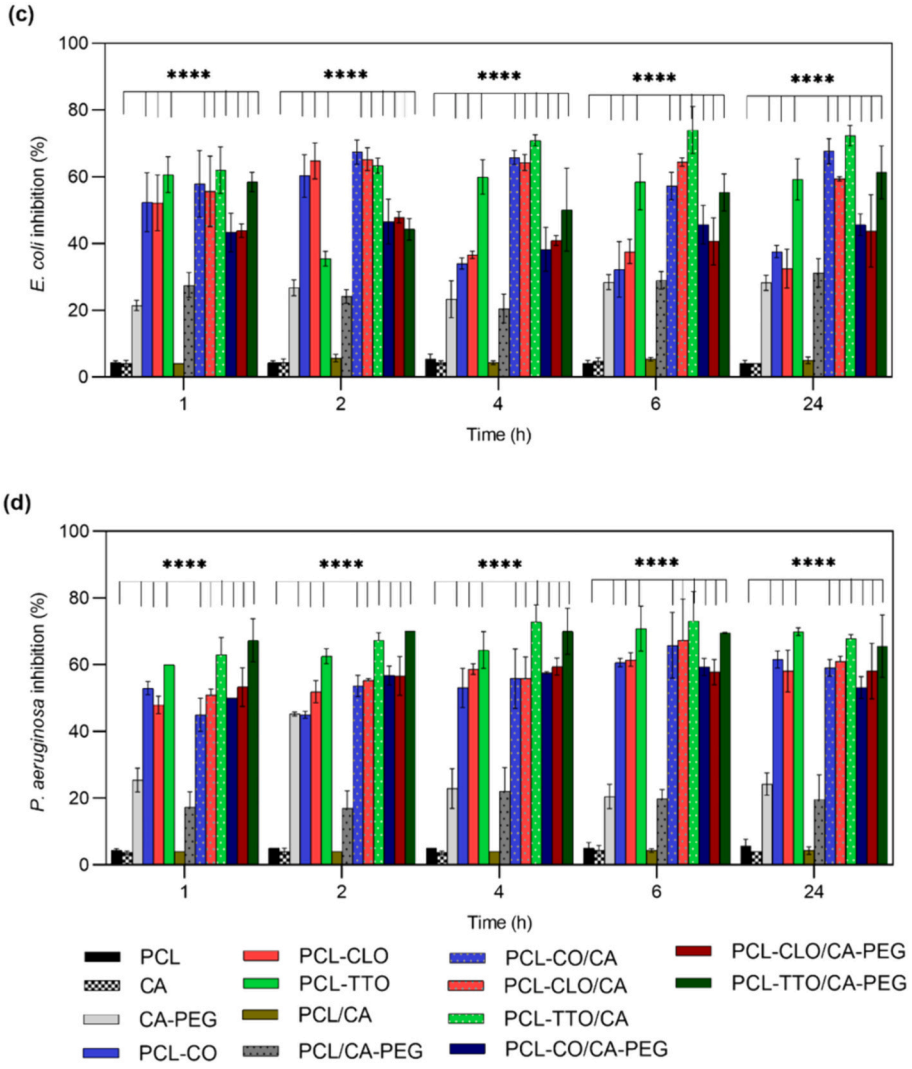

Fig. 9. (*continued*).

P. aeruginosa but not against *S. epidermidis* because of this fact [15]. In addition, superior antibacterial effects were observed against *S. aureus* bacterium than *E. coli* and *P. aeruginosa* (for example, ≈ 31.92 % and ≈ 19.89 % higher reductions, respectively, for PCL-CLO fibers) as the latter are Gram-negative bacteria, which two layers of peptidoglycan and lipid proteins offer better protection against antimicrobial agents [67]. Overall, the results attested to the strong antibacterial properties of CO, CLO and TTO, which were proven effective towards inhibiting four of the most prevalent bacteria in chronic wounds [70].

3.12. Cytocompatibility testing

Metabolic activity and cell lysis tests were performed to assess the cytocompatibility of all wet-spun fiber typologies when put in contact with HaCaT and NIH 3 T3 cell lines, mimicking human skin physiological conditions.. Optimum cell concentrations of HaCaT cells for metabolic activity and cell lysis experiments were determined at 1.5×10^4 cells/well and 8×10^3 cells/well, respectively, while for NIH 3 T3 cells, they were established at 20,000 cells/well and 8000 cells/well, respectively (Fig. S7 in Supporting Information).

After treatment with diverse fiber typologies, HaCaT cells reached metabolic activities above 80 % (Fig. 10a). The presence of EOs in the monolayered fibers (PCL-CO, PCL-CLO and PCL-TTO) caused a slight reduction in their metabolic activity (≈ 10 %). However, such effect was not observed in all EO-loaded coaxial fibers. Here, the shell shielded the cells to an over-exposure of the EOs [60]. In fact, CA, the polymer present at the fibers' shell, is often recognized as a material which is not cytotoxic [71]. As an example, in a research performed by Zhijiang et al., CA and poly(hydroxybutyrate) blend nanofiber scaffolds enhanced cellular adhesion and proliferation [72]. It is also notable to mention that composite scaffolds containing CA, elaborated by Ninan et al., also reached high cytocompatibility levels when exposed to NIH 3 T3 cells [73]. Another important factor explaining the present results is associated with, the superior structural integrity of all fibers when in contact with physiological media (Fig. 6), since a low amount of polymer fragments and/or EOs were released into the media; therefore, not interfering with any relevant biological pathways that dictate the cells survival [19,74]. Another relevant factor is associated with the presence of PCL in the fibers. According to literature, such polymer usually does not induce any cytotoxic effects [75]. For instance, Yaseri et al., using PCL nanofibers, attained ≈ 85 % of cell viability regarding cytocompatibility and proliferation tests on mouse fibroblasts (L929) [76]. Similar results were also acquired with spider silk, gelatin and PCL-containing scaffolds produced by Xiang et al. and PCL-poly(lactide-*co*-glycolide) (PLGA) scaffolds [77,78]. It is also relevant to mention that, due to the hydrophobic nature of PCL, no interferences from any protein adsorption processes were detected, therefore not compromising the metabolic activities of the cells [79,80]. In fact, previous studies have

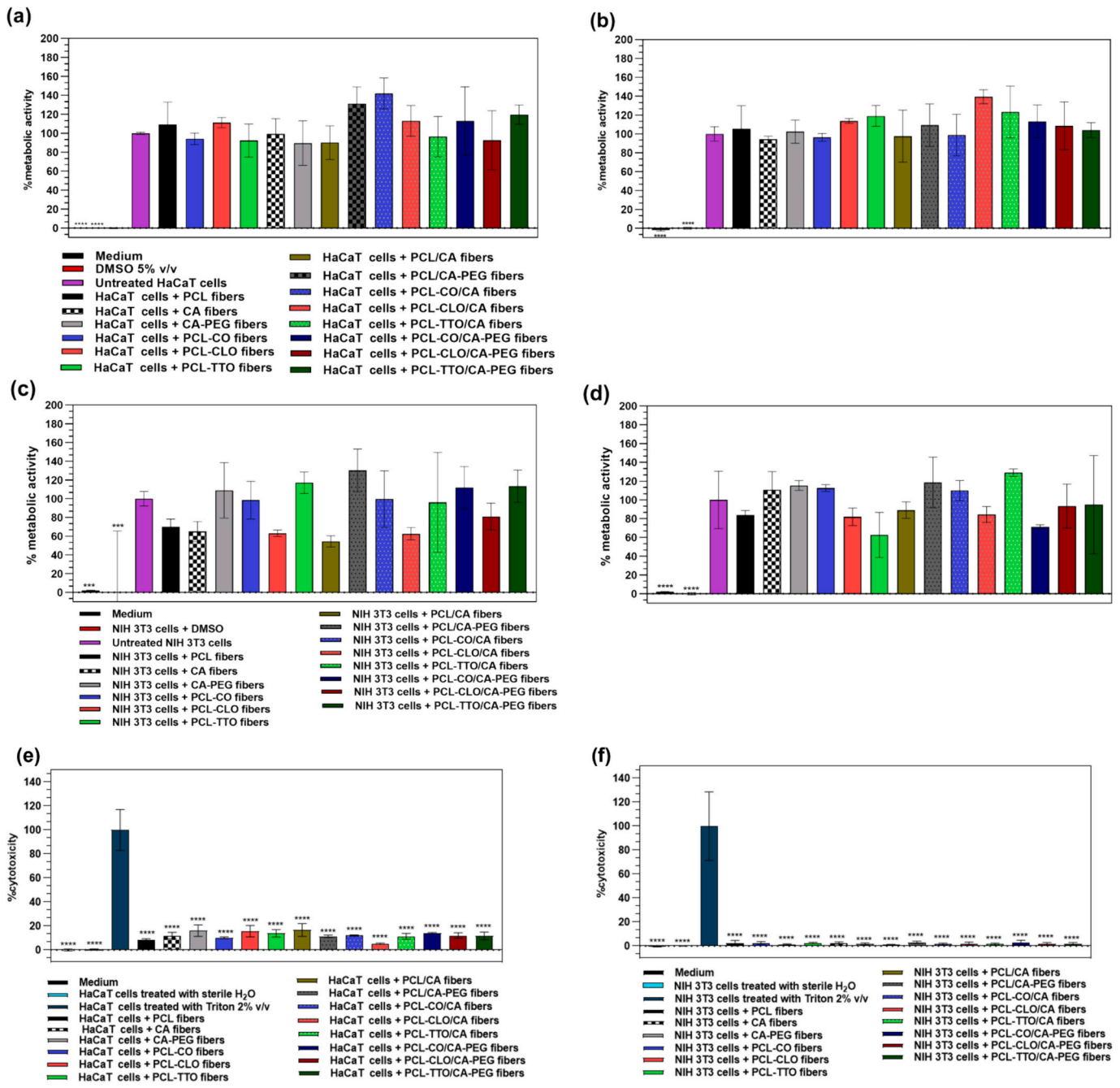

Fig. 10. Cytocompatibility evaluation of HaCaT and NIH 3 T3 cell lines after (a), (c) 24 h and (b), (d) 48 h of contact with fibers, respectively; Cell lysis evaluation of (e) HaCaT and (f) NIH 3 T3 cell lines. Data are reported as mean ± S.D. ($n = 3$). Statistical significance was determined via Dunnett test applying multiple comparisons between the different fiber typologies and each respective positive control (***$p < 0.0007$; ****$p < 0.0001$).

shown similar results, in which the addition of PCL to several types of polymeric structures resulted in higher metabolic activities of cells [74,79]. Additionally, all wet-spun fibers caused low cell lysis (< 20 %) (Fig. 10c) and no changes in cell morphology were observed (Fig. S8 in Supporting Information). The present results attest to the cytocompatibility of the fibers when put in contact with HaCaT since, according to ISO standard 10.93–5:2009, a cytotoxic effect is only established when a reduction of cell viability is higher than 30 %.

NIH 3 T3 cells appeared to be more sensitive to changes in their metabolic activities than HaCaT cells (Fig. 8b). At the 24 h mark, CLO-loaded fibers (PCL-CLO and PCL-CLO/CA) presented metabolic activities lower than 70 %, which is explained by the superior release of CLO from the fibers, compared to TTO and CO (Fig. 7). To the authors' knowledge, the mechanism of action of CLO against NIH 3 T3 cells is not yet fully understood. Nonetheless, the negative effects of such compound against different cell lines have been reported [81–83]. It has been estimated that the toxic effects of CLO may arise from the presence of eugenol and cinnamaldehyde, which exhibit anti-proliferative properties [83]. Hypotheses regarding the mechanism of action of this EO have been proposed by Ahn et al., namely via stimulation of cell death by apoptosis, cell-cycle arrest or the loss of function of relevant cell organelles [81]. However, this effect was no longer detected at the 48 h time-point. In fact, fibers reported an increase in their metabolic activities, demonstrating that NIH 3 T3 cells had the ability to recover from CLO cytotoxic effects. On the other hand, at 48 h, PCL-TTO fibers displayed an activity slightly lower than 70 %, possibly due to the smaller

affinity between PCL and TTO, possibly leading to a release of the EO onto the media in a less controlled manner [13]. It has been shown that TTO displays toxic effects against fibroblast-like cells, inducing the suppression of the interleukin 8 (IL-8) [84,85]. Yet, it was again observed that a shell can guard TTO release to the environment, since the fibers PCL-TTO/CA and PCL-TTO/CA-PEG achieved 129 % and 95 % of metabolic activities, respectively. Indeed, according to several studies involving cytocompatibility tests of TTO-loaded structures, the cytocompatibility of the EO is dependent on its concentration, with low concentrations, not reporting cytotoxic effects on HaCaT [86,87]. Moreover, all wet-spun fibers caused very low cell lysis (Fig. 10d) and no morphological changes in NIH 3 T3 cells (Fig. S9 in Supporting Information). Interestingly, the cells presented a rounded shape, distinct from the common extended shape of fibroblasts. Several researches have reported such occurrence, as NIH 3 T3 morphology changes according to the increase in confluence on which substrate the cells are seeded [88,89].

Despite the slight impact of the EOs on the NIH 3 T3 cells' metabolic activities, the presence of a polymeric shell has supported the cells recover from potential cytotoxic effects. Data showed high cytocompatibility levels for all wet-spun fibers when in contact with both HaCaT and NIH 3 T3 cell lines, attesting to the safety of the fibers for their foreseen application.

4. Conclusion

The development of EOs-loaded coaxial wet-spun fibers is proposed in this research for potential application in chronic wound healing. Indeed, as chronic wounds are often caused by bacterial infections, EOs present great potential due to their effective antibacterial, anti-inflammatory and antioxidant properties. The engineered wet-spun fibers can therefore incorporate such compounds, simultaneously offering protection from surrounding environments and allowing for EOs controlled release. Additionally, the selected polymers PCL, CA and PEG, are endowed with unique properties, making them ideal for biomedical applications, also preserving the structural integrity of the engineered fibers. Indeed, the EO-loaded wet-spun fibers presented high elasticities and maintained their morphologies and structures when exposed to PBS. Notably, the fibrous constructs possessed antioxidant activity and the antibacterial properties, due to the different EOs' successful incorporation onto the fibers. CLO-loaded fibers showed slightly higher release profiles as well as antibacterial and antioxidant properties, in comparison with both CO/TTO-loaded fibers. It is also relevant to mention that the presence of PEG on the fibers' shell did not significantly influence the fibers' biological properties. Cytocompatibility testing revealed the safety of the coaxial wet-spun fibers for their intended application; yet, more experimental work will be required to attest their healing abilities in chronic wounds and inhibitory functions against a wider range of microorganisms, including multi-resistant. Future work will also be required in order to optimize the wet-spun system, enhancing its mechanical properties and the homogeneity of the filaments, approximating its properties to the needs of a future application as a wound dressing.

CRediT authorship contribution statement

Elina Marinho: Writing – review & editing, Investigation. **Catarina Leal Seabra:** Writing – review & editing, Writing – original draft, Investigation, Data curation. **Camille Evenou:** Writing – review & editing, Investigation. **Jérôme Lamartine:** Writing – review & editing, Supervision, Funding acquisition. **Berengere Fromy:** Writing – review & editing, Supervision, Funding acquisition. **Susana P.G. Costa:** Writing – review & editing, Supervision. **Natália C. Homem:** Writing – review & editing, Supervision. **Helena P. Felgueiras:** Writing – review & editing, Supervision, Funding acquisition, Conceptualization.

Declaration of competing interest

The authors declare no conflict of interest.

Acknowledgements

This work was funded by the European Regional Development Fund through the Operational Competitiveness Program and the National Foundation for Science and Technology of Portugal (FCT) under the projects UID/CTM/00264/2020 of Centre for Textile Science and Technology (2C2T) on its components base (https://doi.org/10.54499/UIDB/00264/2020) and programmatic (https://doi.org/10.54499/UIDP/00264/2020). C.S.M. acknowledges FCT for PhD funding via scholarship 2020.08547.BD along with extra funding for conducting an international internship in Lyon. H.P.F. also acknowledges FCT for auxiliary researcher contract 2021.02720.CEEIND (https://doi.org/10.54499/DL57/2016/CP1377/CT0098).

Appendix A. Supplementary data

Supplementary data to this article can be found online at https://doi.org/10.1016/j.ijbiomac.2024.134565.

References

[1] H.P. Felgueiras, M.T.P. Amorim, Functionalization of electrospun polymeric wound dressings with antimicrobial peptides, Colloids Surfaces B Biointerfaces. 156 (2017) 133–148, https://doi.org/10.1016/j.colsurfb.2017.05.001.
[2] K. Rahim, S. Saleha, X. Zhu, L. Huo, A. Basit, O.L. Franco, Bacterial contribution in chronicity of wounds, Microb. Ecol. 73 (2017) 710–721, https://doi.org/10.1007/s00248-016-0867-9.
[3] L.M. Weiner, A.K. Webb, B. Limbago, M.A. Dudeck, J. Patel, A.J. Kallen, J. R. Edwards, D.M. Sievert, Antimicrobial-resistant pathogens associated with healthcare-associated infections: summary of data reported to the National Healthcare Safety Network at the Centers for Disease Control and Prevention, 2011-2014, Infect. Control Hosp. Epidemiol. 37 (2016) 1288–1301, https://doi.org/10.1017/ice.2016.174.
[4] L. Cañedo-Dorantes, M. Cañedo-Ayala, Skin acute wound healing: a comprehensive review, Int. J. Inflam. 2019 (2019), https://doi.org/10.1155/2019/3706315.
[5] M. Bonten, J.R. Johnson, A.H.J. Van Den Biggelaar, L. Georgalis, J. Geurtsen, P. I. De Palacios, S. Gravenstein, T. Verstraeten, P. Hermans, J.T. Poolman, Epidemiology of Escherichia coli bacteremia: a systematic literature review, Clin. Infect. Dis. 72 (2021) 1211–1219, https://doi.org/10.1093/cid/ciaa210.
[6] M.S. Walters, J.E. Grass, S.N. Bulens, E.B. Hancock, E.C. Phipps, D. Muleta, J. Mounsey, M.A. Kainer, C. Concannon, G. Dumyati, C. Bower, J. Jacob, P. M. Cassidy, Z. Beldavs, K. Culbreath, W.E. Phillips, D.J. Hardy, R.L. Vargas, M. Oethinger, U. Ansari, R. Stanton, V. Albrecht, A.L. Halpin, M. Karlsson, J. K. Rasheed, A. Kallen, Carbapenem-resistant pseudomonas aeruginosa at us emerging infections program sites, Emerg. Infect. Dis. 25 (2019) (2015) 1281–1288, https://doi.org/10.3201/eid2507.181200.
[7] Otto, Strategi Implementasi..., Baragina Widyaningrum, Program Pascasarjana, 2008, Nat Rev. Microbiol. 7 (2009) 555–567. doi:https://doi.org/10.1038/nrmicro2182.Staphylococcus.
[8] Report on the Burden of Endemic Health Care-Associated Infection Worldwide Clean Care is Safer Care, (n.d.).
[9] M. Applications, Microbial Systematics Biomolecules and Natural Macromolecules Applications, n.d.
[10] C.S. Miranda, J.C. Antunes, N.C. Homem, H.P. Felgueiras, Controlled Release of Cinnamon Leaf Oil from Chitosan Microcapsules Embedded within a Sodium Alginate/Gelatin Hydrogel-Like Film for *Pseudomonas aeruginosa* Elimination, (2021) 7181. doi:https://doi.org/10.3390/cgpm2020-07181.
[11] H.P. Felgueiras, N.C. Homem, M.A. Teixeira, A.R.M. Ribeiro, J.C. Antunes, M.T. P. Amorim, Physical, thermal, and antibacterial effects of active essential oils with potential for biomedical applications loaded onto cellulose acetate/polycaprolactone wet-spun microfibers, Biomolecules 10 (2020) 1–20, https://doi.org/10.3390/biom10081129.
[12] T.D. Tavares, J.C. Antunes, F. Ferreira, H.P. Felgueiras, Biofunctionalization of natural Fiber-reinforced biocomposites for biomedical Applications, Biomolecules 10 (2020), https://doi.org/10.3390/biom10010148.
[13] J.C. Antunes, T.D. Tavares, M.A. Teixeira, M.O. Teixeira, N.C. Homem, M.T. P. Amorim, H.P. Felgueiras, Eugenol-containing essential oils loaded onto chitosan/polyvinyl alcohol blended films and their ability to eradicate staphylococcus aureus or pseudomonas aeruginosa from infected microenvironments, Pharmaceutics 13 (2021), https://doi.org/10.3390/pharmaceutics13020195.
[14] R. Kamel, S.M. Afifi, A.M. Abdou, T. Esatbeyoglu, M.M. AbouSamra, Nanolipogel loaded with tea tree oil for the Management of Burn: GC-MS analysis, in vitro and

in vivo evaluation, Molecules 27 (2022) 1–19, https://doi.org/10.3390/molecules27196143.
[15] M. Hameed, A. Rasul, M.K. Waqas, M. Saadullah, N. Aslam, G. Abbas, S. Latif, H. Afzal, S. Inam, P.A. Shah, Formulation and evaluation of a clove oil-encapsulated nanofiber formulation for effective wound-healing, Molecules 26 (2021), https://doi.org/10.3390/molecules26092491.
[16] J. Wang, Y. Li, Y. Gao, Z. Xie, M. Zhou, Y. He, H. Wu, W. Zhou, X. Dong, Z. Yang, Y. Hu, Cinnamon oil-loaded composite emulsion hydrogels with antibacterial activity prepared using concentrated emulsion templates, Ind. Crop. Prod. 112 (2018) 281–289, https://doi.org/10.1016/j.indcrop.2017.12.022.
[17] Y. Ge, M. Ge, Development of tea tree oil-loaded liposomal formulation using response surface methodology, J. Liposome Res. 25 (2015) 222–231, https://doi.org/10.3109/08982104.2014.987786.
[18] C.S. Miranda, A.F.G. Silva, S.M.M.A. Pereira-Lima, S.P.G. Costa, N.C. Homem, H. P. Felgueiras, Tunable spun Fiber constructs in biomedicine: influence of processing parameters in the Fibers' architecture, Pharmaceutics 14 (2022), https://doi.org/10.3390/pharmaceutics14010164.
[19] A. Mirabedini, Developing Novel Spinning Methods to Fabricate Continuous Multifunctional Fibres for A thesis submitted in the fulfilment of the, (2017) 1–235.
[20] M.A. Teixeira, M.C. Paiva, M.T.P. Amorim, H.P. Felgueiras, Electrospun nanocomposites containing cellulose and its derivatives modified with specialized biomolecules for an enhanced wound healing, Nanomaterials 10 (2020), https://doi.org/10.3390/nano10030557.
[21] I.R. Calori, G. Braga, P. da C.C. de Jesus, H. Bi, A.C. Tedesco, Polymer scaffolds as drug delivery systems, Eur. Polym. J. 129 (2020) 109621, https://doi.org/10.1016/j.eurpolymj.2020.109621.
[22] C.S. Miranda, A.R.M. Ribeiro, N.C. Homem, H.P. Felgueiras, Spun Biotextiles in Tissue Engineering and Biomolecules Delivery Systems (2020), https://doi.org/10.3390/antibiotics9040174.
[23] T. Thanh, H. Thi, E.H. Pilkington, D.H. Nguyen, J.S. Lee, The Importance of Poly (Ethylene Glycol) Alternatives for Overcoming PEG Immunogenicity in Drug, (n. d.).
[24] S. Sun, Y. Cui, B. Yuan, M. Dou, G. Wang, Drug delivery systems based on polyethylene glycol hydrogels for enhanced bone regeneration (2023) 1–17, https://doi.org/10.3389/fbioe.2023.1117647.
[25] P. Matzinos, V. Tserki, A. Kontoyiannis, C. Panayiotou, Processing and characterization of starch/polycaprolactone products, Polym. Degrad. Stab. 77 (2002) 17–24, https://doi.org/10.1016/S0141-3910(02)00072-1.
[26] M.G.A. Vieira, M.A. Da Silva, L.O. Dos Santos, M.M. Beppu, Natural-based plasticizers and biopolymer films: a review, Eur. Polym. J. 47 (2011) 254–263, https://doi.org/10.1016/j.eurpolymj.2010.12.011.
[27] I. Wiegand, K. Hilpert, R.E.W. Hancock, Agar and broth dilution methods to determine the minimal inhibitory concentration (MIC) of antimicrobial substances, Nat. Protoc. 3 (2008) 163–175, https://doi.org/10.1038/nprot.2007.521.
[28] European Society of Clinical Microbiology and Infectious Diseases, Broth Dilution, Clin. Microbiol. Infect. 9 (2003) (2003) 1–7.
[29] C. Sebaaly, A. Jraij, H. Fessi, C. Charcosset, H. Greige-Gerges, Preparation and characterization of clove essential oil-loaded liposomes, Food Chem. 178 (2015) 52–62, https://doi.org/10.1016/j.foodchem.2015.01.067.
[30] N.A. Zabidi, F. Nazri, I. Syafinaz, M. Amin, M. Salahuddin, M. Basri, R.K. Basha, S. H. Othman, Jo ur na l P, Int. J. Biol. Macromol. 2 (2022) 33–47, https://doi.org/10.1016/j.bioadv.2023.213488.
[31] M. Koli, S. Kmiecik, P. Roszkowski, J. Szyma, M. Struga, D. Szulczyk, Novel Tetrazole-Based Antimicrobial Agents Targeting Clinical Bacteria Strains: Exploring the Inhibition of Staphylococcus aureus DNA Topoisomerase IV and Gyras, Int. J. Mol. Sci. 23 (2022) 378–392.
[32] M. Chen, Y. Hu, J. Zhou, Y. Xie, H. Wu, T. Yuan, Z. Yang, Facile fabrication of tea tree oil-loaded antibacterial microcapsules by complex coacervation of sodium alginate/quaternary ammonium salt of chitosan, RSC Adv. 6 (2016) 13032–13039, https://doi.org/10.1039/c5ra26052c.
[33] A. Akturk, Enrichment of cellulose acetate Nanofibrous scaffolds with Retinyl palmitate and clove essential oil for wound healing Applications, ACS Omega 8 (2023) 5553–5560, https://doi.org/10.1021/acsomega.2c06881.
[34] S. Majumder, M.A. Matin, A. Sharif, M.T. Arafat, Electrospinning of antibacterial cellulose acetate/polyethylene glycol fiber with in situ reduced silver particles, J. Polym. Res. 27 (2020), https://doi.org/10.1007/s10965-020-02356-2.
[35] C. Chen, L. Wang, Y. Huang, Electrospun phase change fibers based on polyethylene glycol/cellulose acetate blends, Appl. Energy 88 (2011) 3133–3139, https://doi.org/10.1016/j.apenergy.2011.02.026.
[36] N.C. Homem, T.D. Tavares, C.S. Miranda, J.C. Antunes, M.P. Teresa, H.P. Felgueiras, Functionalization of crosslinked sodium alginate / gelatin wet-spun porous fibers with Nisin Z for the inhibition of *Staphylococcus aureus* - induced infections, (n.d.).
[37] I. Unalan, S.J. Endlein, B. Slavik, A. Buettner, W.H. Goldmann, R. Detsch, A. R. Boccaccini, Evaluation of electrospun poly(ε-caprolactone)/gelatin nanofiber mats containing clove essential oil for antibacterial wound dressing, Pharmaceutics 11 (2019), https://doi.org/10.3390/pharmaceutics11110570.
[38] K. Khoshnevisan, H. Maleki, H. Samadian, M. Doostan, M.R. Khorramizadeh, Antibacterial and antioxidant assessment of cellulose acetate/polycaprolactone nanofibrous mats impregnated with propolis, Int. J. Biol. Macromol. 140 (2019) 1260–1268, https://doi.org/10.1016/j.ijbiomac.2019.08.207.
[39] C.S. Miranda, A.F.G. Silva, C.L. Seabra, S. Reis, M.M.P. Silva, S.M.M.A. Pereira-lima, S.P.G. Costa, H.P. Felgueiras, Sodium alginate / polycaprolactone co-axial wet-spun microfibers modified with N-carboxymethyl chitosan and the peptide AAPV for *Staphylococcus aureus* and human neutrophil elastase i ... Biomaterials Advances Sodium alginate / polycaprolactone co-axial wet-spun microfibers modified with N -carboxymethyl chitosan and the peptide AAPV for *Staphylococcus aureus* and human neutrophil elastase inhibition in potential chronic wound scenarios, (2023). doi:https://doi.org/10.1016/j.bioadv.2023.213488.
[40] A. Benkaddour, K. Jradi, S. Robert, C. Daneault, Grafting of polycaprolactone on oxidized nanocelluloses by click chemistry, Nanomaterials 3 (2013) 141–157, https://doi.org/10.3390/nano3010141.
[41] P. Fei, L. Liao, B. Cheng, J. Song, Quantitative analysis of cellulose acetate with a high degree of substitution by FTIR and its application, Anal. Methods 9 (2017) 6194–6201, https://doi.org/10.1039/c7ay02165h.
[42] X. He, Optimization of deacetylation process for regenerated cellulose hollow Fiber membranes, Int. J. Polym. Sci. 2017 (2017), https://doi.org/10.1155/2017/3125413.
[43] J.M. Domingues, M.O. Teixeira, M.A. Teixeira, D. Freitas, S.F. da Silva, S.D. Tohidi, R.D.V. Fernandes, J. Padrão, A. Zille, C. Silva, J.C. Antunes, H.P. Felgueiras, Inhibition of Escherichia virus MS2, surrogate of SARS-CoV-2, via essential oils-loaded electrospun fibrous Mats: increasing the multifunctionality of antivirus protection masks, Pharmaceutics 14 (2022), https://doi.org/10.3390/pharmaceutics14020303.
[44] S. Zhelyazkov, G. Zsivanovits, E. Stamenova, M. Marudova, Physical and barrier properties of clove essential oil loaded potato starch edible films, Biointerface Res. Appl. Chem. 12 (2022) 4603–4612, https://doi.org/10.33263/BRIAC124.46034612.
[45] S. Phaiju, P. Mulmi, D.K. Shahi, T.I. Hwang, A.P. Tiwari, R. Joshi, H.R. Pant, M. K. Joshi, Antibacterial cinnamon essential oil incorporated poly(Ɛ−Caprolactone) Nanofibrous Mats: new platform for biomedical application, J. Inst. Sci. Technol. 25 (2020) 9–16, https://doi.org/10.3126/jist.v25i2.33724.
[46] S.D. Ribeiro, A.B. Meneguin, H. da S. Barud, J.M. Silva, R.L. Oliveira, R.M.N. de Asunção, T.F. Tormin, R.A.A. Muñoz, G.R. Filho, C.A. Ribeiro, Synthesis and characterization of cellulose acetate from cellophane industry residues. Application as acetaminophen controlled-release membranes, J. Therm. Anal. Calorim. 147 (2022) 7265–7275, https://doi.org/10.1007/s10973-021-11022-8.
[47] P.A. Vinodhini, K. Sangeetha, G. Thandapani, P.N. Sudha, V. Jayachandran, A. Sukumaran, FTIR, XRD and DSC studies of nanochitosan, cellulose acetate and polyethylene glycol blend ultrafiltration membranes, Int. J. Biol. Macromol. 104 (2017) 1721–1729, https://doi.org/10.1016/j.ijbiomac.2017.03.122.
[48] R.F. Faradilla, G. Lee, P. Sivakumar, M. Stenzel, J. Arcot, Effect of polyethylene glycol (PEG) molecular weight and nanofillers on the properties of banana pseudostem nanocellulose films, Carbohydr. Polym. 205 (2019) 330–339, https://doi.org/10.1016/j.carbpol.2018.10.049.
[49] X. Zhan, R. Ge, S. Yao, J. Lu, X. Sun, J. Li, Enhanced pervaporation performance of PEG membranes with synergistic effect of cross-linked PEG and porous MOF-508a, Sep. Purif. Technol. 304 (2023) 122347, https://doi.org/10.1016/j.seppur.2022.122347.
[50] H.M. Ng, F.S. Omar, R. Kasi, Thermogravimetric Analysis of Polymers (2018), https://doi.org/10.1002/0471440264.pst667.
[51] P. Nezhad-mokhtari, H. Hamishehkar, M.R. Farahpour, Engineered bioadhesive self-healing nanocomposite hydrogel to fight infection and accelerate cutaneous wound healing, Chem. Eng. J. 489 (2024) 150992, https://doi.org/10.1016/j.cej.2024.150992.
[52] E.M. Abdelrazek, A.M. Hezma, A. El-khodary, A.M. Elzayat, Spectroscopic studies and thermal properties of PCL/PMMA biopolymer blend, Egypt. J. Basic Appl. Sci. 3 (2016) 10–15, https://doi.org/10.1016/j.ejbas.2015.06.001.
[53] M. De Carvalho Eufrásio Pinto, D. David Da Silva, A.L. Amorim Gomes, V. dos S.A. Leite, A.R. Fialho E Moraes, R. Ferreira de Novais, J. Tronto, F.G. Pinto, Film based on magnesium impregnated biochar/cellulose acetate for phosphorus adsorption from aqueous solution, RSC Adv. 9 (2019) 5620–5627. doi:https://doi.org/10.1039/c8ra06655h.
[54] S.K. Kwon, D.H. Kim, Effect of process parameters of UV-assisted gas-phase cleaning on the removal of PEG (polyethyleneglycol) from a Si substrate, J. Korean Phys. Soc. 49 (2006) 1421–1427.
[55] T.L.A. Montanheiro, L.S. Montagna, M.A. de Farias, J.A. Magalhães, D.B. Tada, F. R. Passador, J.P.B. Machado, A.P. Lemes, Cytotoxicity and physico-chemical evaluation of acetylated and pegylated cellulose nanocrystals, J. Nanopart. Res. 20 (2018), https://doi.org/10.1007/s11051-018-4306-3.
[56] X. Dreux, C. Carrot, A. Argoud, C. Vergelati, Viscoelastic behaviour of cellulose acetate / triacetin blends by rheology in the melt state (2019) 1–19.
[57] G.U. Rani, S. Sharma, Biopolymers, Bioplastics and Biodegradability: An Introduction, in: Ref. Modul. Mater. Sci. Mater. Eng., Elsevier, 2021. doi:doi: https://doi.org/10.1016/B978-0-12-820352-1.00131-0.
[58] C.D. Grande-Tovar, J.I. Castro, C.H. Valencia Llano, D.L. Tenorio, M. Saavedra, P. A. Zapata, M.N. Chaur, Polycaprolactone (PCL)-Polylactic acid (PLA)-glycerol (Gly) composites incorporated with zinc oxide nanoparticles (ZnO-NPs) and tea tree essential oil (TTEO), for Tissue Engineering Applications, Pharmaceutics 15 (2023), https://doi.org/10.3390/pharmaceutics15010043.
[59] S. Chew, Y. Wen, Y. Dzenis, K. Leong, The role of electrospinning in the emerging field of nanomedicine, Curr. Pharm. Des. 12 (2006) 4751–4770, https://doi.org/10.2174/138161206779026326.
[60] A. Li, I.N. Khan, I.U. Khan, A.M. Yousaf, Y. Shahzad, Gellan gum-based bilayer mucoadhesive films loaded with moxifloxacin hydrochloride and clove oil for possible treatment of periodontitis, Drug Des. Devel. Ther. 15 (2021) 3937–3952, https://doi.org/10.2147/DDDT.S328722.
[61] A. Huang, Y. Jiang, B. Napiwocki, H. Mi, X. Peng, L.S. Turng, Fabrication of poly (ε-caprolactone) tissue engineering scaffolds with fibrillated and interconnected pores utilizing microcellular injection molding and polymer leaching, RSC Adv. 7 (2017) 43432–43444, https://doi.org/10.1039/c7ra06987a.

[62] M. Fornazier, P.G. De Melo, D. Pasquini, H. Otaguro, Additives Incorporated in Cellulose Acetate Membranes to Improve Its Performance as a Barrier in Periodontal Treatment 2 (2021) 1–9, https://doi.org/10.3389/fdmed.2021.776887.
[63] B. Werbner, M. Zhou, N. Mcmindes, A. Lee, M. Lee, G.D.O. Connell, Journal of the mechanical behavior of biomedical materials saline-polyethylene glycol blends preserve in vitro annulus fibrosus hydration and mechanics : an experimental and finite-element analysis, J. Mech. Behav. Biomed. Mater. 125 (2022) 104951, https://doi.org/10.1016/j.jmbbm.2021.104951.
[64] W. Cui, X. Zhu, Y. Yang, X. Li, Y. Jin, Evaluation of electrospun fibrous scaffolds of poly(dl-lactide) and poly(ethylene glycol) for skin tissue engineering, Mater. Sci. Eng. C 29 (2009) 1869–1876, https://doi.org/10.1016/j.msec.2009.02.013.
[65] A.H. Shamsah, S.H. Cartmell, S.M. Richardson, L.A. Bosworth, Material characterization of PCL:PLLA electrospun fibers following six months degradation in vitro, Polymers (Basel). 12 (2020) 1–11, https://doi.org/10.3390/polym12030700.
[66] L. Moradkhannejhad, M. Abdouss, N. Nikfarjam, M.H. Shahriari, V. Heidary, The effect of molecular weight and content of PEG on in vitro drug release of electrospun curcumin loaded PLA/PEG nanofibers, J. Drug Deliv. Sci. Technol. 56 (2020) 101554, https://doi.org/10.1016/j.jddst.2020.101554.
[67] Y. Jung, H. Yang, I.-Y. Lee, T.-S. Yong, S. Lee, Polymers containing cinnamon oil : their antibacterial and antifungal properties and Acaricidal E ff ect against house dust mites, Polymers (Basel). 12 (2020) 1–18.
[68] R. Btissam, R. Rajae, A. Amina, V. Brigitte, In vitro study of anti-glycation and radical scavenging activities of the essential oils of three plants from Morocco : Origanum compactum, *Rosmarinus officinalis* and Pelargonium asperum 7 (2015), https://doi.org/10.5530/pj.2015.2.7.
[69] G.I. Ndukwe, M.N. Ighomuaye, CHEMICAL COMPOSITION AND IN VITRO ANTIMICROBIAL ACTIVITY OF ESSENTIAL OILS OF *Jatropha CURCAS* LINN . (EUPHORBIACEAE), (2018).
[70] B.A.R.N. Durand, C. Pouget, C. Magnan, V. Molle, J.P. Lavigne, C. Dunyach-Remy, Bacterial interactions in the context of chronic wound biofilm: a review, Microorganisms 10 (2022) 1–18, https://doi.org/10.3390/microorganisms10081500.
[71] E. Esmaeili, T. Eslami-Arshaghi, S. Hosseinzadeh, E. Elahirad, Z. Jamalpoor, S. Hatamie, M. Soleimani, The biomedical potential of cellulose acetate/polyurethane nanofibrous mats containing reduced graphene oxide/silver nanocomposites and curcumin: antimicrobial performance and cutaneous wound healing, Int. J. Biol. Macromol. 152 (2020) 418–427, https://doi.org/10.1016/j.ijbiomac.2020.02.295.
[72] C. Zhijiang, X. Yi, Y. Haizheng, J. Jia, Y. Liu, Poly (hydroxybutyrate)/ cellulose acetate blend nano fi ber scaffolds : Preparation , characterization and cytocompatibility, 58 (2016) 757–767. doi:https://doi.org/10.1016/j.msec.2015.09.048.
[73] N. Ninan, M. Muthiah, I. Park, A. Elain, S. Thomas, Y. Grohens, Pectin / carboxymethyl cellulose / microfibrillated cellulose composite scaffolds for tissue engineering, Carbohydr. Polym. 98 (2013) 877–885, https://doi.org/10.1016/j.carbpol.2013.06.067.
[74] C.S. Miranda, A.F.G. Silva, C.L. Seabra, S. Reis, M.M.P. Silva, S.M.M.A. Pereira-Lima, S.P.G. Costa, N.C. Homem, H.P. Felgueiras, Sodium alginate/polycaprolactone co-axial wet-spun microfibers modified with N-carboxymethyl chitosan and the peptide AAPV for Staphylococcus aureus and human neutrophil elastase inhibition in potential chronic wound scenarios, Biomater. Adv. 151 (2023), https://doi.org/10.1016/j.bioadv.2023.213488.
[75] N. Siddiqui, B. Kishori, S. Rao, M. Anjum, V. Hemanth, S. Das, E. Jabbari, Electropsun Polycaprolactone Fibres in bone tissue engineering : a review, Mol. Biotechnol. 63 (2021) 363–388, https://doi.org/10.1007/s12033-021-00311-0.
[76] R. Yaseri, M. Fadaie, E. Mirzaei, H. Samadian, A. Ebrahiminezhad, Surface modification of polycaprolactone nanofibers through hydrolysis and aminolysis : a comparative study on structural characteristics , mechanical properties , and cellular performance, Sci. Rep. (2023) 1–17. doi:https://doi.org/10.1038/s41598-023-36563-w.
[77] P. Xiang, M. Li, C. Zhang, D. Chen, Z. Zhou, International journal of biological macromolecules Cytocompatibility of electrospun nanofiber tubular scaffolds for small diameter tissue engineering blood vessels, Int. J. Biol. Macromol. 49 (2011) 281–288, https://doi.org/10.1016/j.ijbiomac.2011.05.004.
[78] N. Thi, H.B. Lee, Electro-spinning of PLGA / PCL blends for tissue engineering and their biocompatibility (2010) 1969–1978, https://doi.org/10.1007/s10856-010-4048-y.
[79] W.W. Hu, Y.C. Wu, Z.C. Hu, The development of an alginate/polycaprolactone composite scaffold for in situ transfection application, Carbohydr. Polym. 183 (2018) 29–36, https://doi.org/10.1016/j.carbpol.2017.11.030.
[80] H.P. Felgueiras, N.S. Murthy, S.D. Sommerfeld, M.M. Brás, V. Migonney, J. Kohn, Competitive adsorption of plasma proteins using a quartz crystal microbalance, ACS Appl. Mater. Interfaces 8 (2016) 13207–13217, https://doi.org/10.1021/acsami.5b12600.
[81] C. Ahn, J.A.E.H. Lee, M.I.J.I.N. Park, J.A.E.W.O.O. Kim, J. Yang, Y.M.I.N. Yoo, E.U. I.B.A.E. Jeung, Cytostatic effects of plant essential oils on human skin and lung cells, (2020) 2008–2018. doi:https://doi.org/10.3892/etm.2020.8460.
[82] W. Prabhashini, K. Mendis, G. Arachchige, S. Premakumara, Anti - inflammatory , cytotoxicity and antilipidemic properties : novel bioactivities of true cinnamon (*Cinnamomum zeylanicum* Blume) leaf, BMC Complement. Med. Ther. 5 (2022) 1–15. doi:https://doi.org/10.1186/s12906-022-03728-5.
[83] T. Huang, H. Chi-tang, F. Hui-yin, Cytotoxic Properties of Leaf Essential Oil and Components from Indigenous Cinnamon (Cinnamomum osmophloeum Kaneh) (2006) 299–313.
[84] A. Thor, A. Johanssonb, R. Grefc, Toxic effects of some conifer resin acids and tea tree oil on human epithelial and fibroblast cells 107 (1996) 99–109.
[85] G. Ramage, S. Milligan, D.F. Lappin, L. Sherry, P. Sweeney, C. Williams, J. Bagg, S. Culshaw, Antifungal , cytotoxic , and immunomodulatory properties of tea tree oil and its derivative components : potential role in management of oral candidosis in cancer patients, 3 (2012) 1–8. doi:https://doi.org/10.3389/fmicb.2012.00220.
[86] D.C. Homeyer, C.J. Sanchez, K. Mende, M.L. Beckius, C.K. Murray, J.C. Wenke, K.S. Akers, In Vitro activity of Melaleuca alternifolia (tea tree) oil on filamentous fungi and toxicity to human cells, (2015) 1–10. doi:https://doi.org/10.1093/mmy/myu072.
[87] L. Ultrastrutture, Ã. Laboratorio, T. Comparata, I. Superiore, A. Calcabrini, A. Stringaro, L. Toccacieli, S. Meschini, M. Marra, M. Colone, G.S. Ã, F. Mondello, G. Arancia, A. Molinari, Terpinen-4-ol , The Main Component of Melaleuca Alternifolia (Tea Tree) Oil Inhibits the In Vitro Growth of Human Melanoma Cells, (2004).
[88] C.M.P. Ribeiro, J. Reece, J.W. Putney, Role of the cytoskeleton in calcium signaling in NIH 3T3 cells - An intact cytoskeleton is required for agonist-induced [Ca2 +](i) signaling , but not for capacitative calcium entry Role of the Cytoskeleton in Calcium Signaling in NIH 3T3 Cells, (2016). doi:https://doi.org/10.1074/jbc.272.42.26555.
[89] A.M. Rahimi, M. Cai, S. Hoyer-fender, Heterogeneity of the NIH3T3 Fibroblast Cell Line, 2022.